

# Geochemistry, Geophysics, Geosystems

## RESEARCH ARTICLE

10.1029/2018GC007987

### Key Points:

- Based on  $^3\text{He}/^4\text{He}$ , the gases emitted from the Baja California Peninsula have two origins: magmatic and hydrothermal
- The hydrothermal gases contain variable mantle contributions that indicate the presence of active faults
- The mantle beneath the Baja California Peninsula could be contaminated from subducted C-rich sediment

### Supporting Information:

- Supporting Information S1
- Table S1
- Table S2

### Correspondence to:

R. Y. Batista Cruz,  
rbatista@cicese.edu.mx

### Citation:

Batista Cruz, R. Y., Rizzo, A. L., Grassa, F., Bernard Romero, R., González Fernández, A., Kretzschmar, T. G., & Gómez-Arias, E. (2019). Mantle degassing through continental crust triggered by active faults: The case of the Baja California Peninsula, Mexico. *Geochemistry, Geophysics, Geosystems*, 20. <https://doi.org/10.1029/2018GC007987>


Received 25 OCT 2018

Accepted 9 MAR 2019

Accepted article online 14 MAR 2019

©2019. American Geophysical Union.  
All Rights Reserved.

## Mantle Degassing Through Continental Crust Triggered by Active Faults: The Case of the Baja California Peninsula, Mexico

Ramón Yosvanis Batista Cruz<sup>1</sup> , Andrea Luca Rizzo<sup>2</sup> , Fausto Grassa<sup>2</sup> , Rubén Bernard Romero<sup>3</sup> , Antonio González Fernández<sup>1</sup> , Thomas Gunter Kretzschmar<sup>1</sup>, and Efraín Gómez-Arias<sup>4</sup> 

<sup>1</sup>Centro de Investigación Científica y de Educación Superior de Ensenada (CICESE), Ensenada, Mexico, <sup>2</sup>Istituto Nazionale di Geofisica e Vulcanologia, Sezione di Palermo, Palermo, Italy, <sup>3</sup>Instituto Nacional de Electricidad y Energías Limpias, Cuernavaca, Cuernavaca, Mexico, <sup>4</sup>CONACYT-Centro de Investigación Científica y de Educación Superior de Ensenada, Ensenada, Mexico

**Abstract** In this work, we report new chemical and isotopic data ( $^3\text{He}/^4\text{He}$ ,  $\delta^{13}\text{C}_{\text{CO}_2}$ ,  $\delta^{13}\text{C}_{\text{CH}_4}$ , and  $\delta\text{D}_{\text{CH}_4}$ ) from poorly or previously unstudied hydrothermal and magmatic gases that are emitted along the eastern coast of the Baja California Peninsula (BCP). High  $^3\text{He}/^4\text{He}$  values (up to  $\sim 7$  Ra) characterize the magmatic gases, while lower ratios ( $\leq 1.6$  Ra) characterize hydrothermal springs. We infer that the mantle beneath the BCP could be Mid-ocean-ridge basalt (MORB)-likes, as in the rift within the Gulf of California, or it may reflect contamination from C-rich sediment during paleo-subduction of the Farallon plate. During their ascent, through the crust, mantle/magmatic gases mix with  $\text{CO}_2$ - and  $^4\text{He}$ -rich fluids, thus forming  $\text{CO}_2$ -rich hydrothermal gases. These hydrothermal gases undergo partial dissolution of  $\text{CO}_2$  in shallow waters under different temperature and pH conditions, which further modifies their composition. Thermogenic and possibly abiogenic sources of methane are present only in magmatic gases from the BCP. Secondary methane oxidation (microbial/inorganic) processes are proposed for some hydrothermal gases, which are extremely enriched in heavy isotopes. Finally, we argue that the hydrothermal gases that are emitted from the BCP have variable percentages of mantle contribution, indicating the presence of lithospheric faults enhancing the rise of mantle fluids also in areas where volcanism is absent.

### 1. Introduction

The release of volatiles from the Earth's interior is a manifestation of its degassing (Anderson, 2007; Fanale, 1971; Hilton et al., 2002; Moreira, 2013), which has been occurring since its formation (Condie, 2005; Tajika, 1998). This degassing is normally present in environments where magmatic activity is present but may occur even in areas where volcanic activity is absent and an active geothermal regime exists (Caracausi et al., 2005; Caracausi & Paternoster, 2015; Giggenbach, 1992; Inguaggiato et al., 2016; Mamyryn & Tolstikhin, 1984; Poreda & Craig, 1989; Umeda et al., 2007). In this respect, the role of active faults and high-seismicity areas in degassing through continental crust constitutes an important scientific debate (Caracausi et al., 2005; Caracausi & Paternoster, 2015; Gülec et al., 2002; Wakita et al., 1987).

Gas chemistry, specifically noble gases and  $\text{CO}_2$  and  $\text{CH}_4$  isotopes, represent excellent natural tracers to evaluate the origin of volatiles and the relationship between active tectonic and magmatic activity (e.g., Caracausi & Paternoster, 2015; Graham, 2002; Kurz et al., 1982; Moreira & Allègre, 1998; Moreira & Sarda, 2000; Rizzo et al., 2015, 2016; Sano & Marty, 1995). Helium has two stable isotopes,  $^3\text{He}$  and  $^4\text{He}$ , whose ratio is useful to distinguish crustal from mantle sources.  $^3\text{He}$  is primordial, not renewed, and stored in the Earth's interior, while  $^4\text{He}$  is radiogenic and continuously produced from the decay of U, Th, and (less significantly) Sm (Moreira, 2013).  $^3\text{He}/^4\text{He}$  is commonly normalized to the same ratio in the atmosphere, which equals  $1.39 \cdot 10^{-6}$  (denoted as Ra, Clarke et al., 1976; Mabry et al., 2013; Mamyryn et al., 1970; Sano et al., 2008). Continental crust is characterized by  $^3\text{He}/^4\text{He}$  ratios from 0.01 to 0.05 Ra (Morrison & Pine, 1955), while Mid-ocean-ridge basalt (MORB) has ratios of  $8 \pm 1$  Ra (Graham, 2002). Thus, excluding any atmospheric input, values above the typical crustal ratio indicate a magmatic or mantle contribution (Ozima & Podosek, 1983). The isotope compositions of  $\text{CO}_2$  and  $\text{CH}_4$  are successfully utilized to define their different

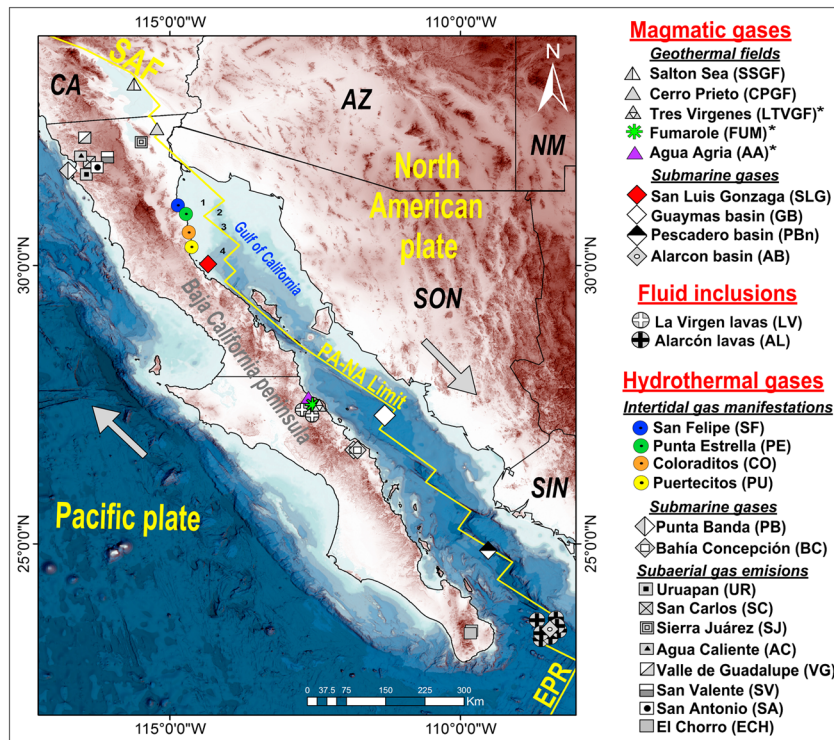


**Figure 1.** Location map of gas emissions and volcanic rocks that were studied for noble gases in the BCP and GoC, distinguished by the typology. The colored symbols correspond to the gas emissions that were sampled in this study. The Las Tres Virgenes geothermal field, Agua Agria, and Fumarole have an asterisk because they belong to the Las Tres Virgenes Volcanic Zone (LTVVZ). The uncolored symbols are gas emissions and volcanic rocks that were previously investigated by the following authors: SSGF from Welhan (1981) and Mazzini et al. (2011); CPGF from Truesdell et al. (1978), Welhan et al. (1978), Polyak et al. (1982), Mazor and Truesdell (1984), Des Marais et al. (1988), Birkle et al. (2016), Pinti et al. (2018), and Richard et al. (2019); LTVGZ from Birkle et al. (2016) and Richard et al. (2019); LV from Schmitt et al. (2010); GB from Lupton (1979), Galimov and Simoneit (1982), and Welhan and Lupton (1987); PBn and AB from Spelz et al. (2015); AL from Castillo et al. (2002); PB, SC, and UR from Vidal et al. (1981), Vidal et al. (1982), and Polyak et al. (1991); UR, AC, SC, SV, VG, SA, and ECH from Polyak et al. (1991); SJ and PU from Negrete-Aranda et al. (2015); and BC from Forrest et al. (2005). In the map, CA, California; AZ, Arizona; NM, New Mexico; SON, Sonora; SIN, Sinaloa. SAF and EPR represent the San Andreas fault and East Pacific Rise, respectively. Numbers: 1, Roca Consag; 2, Wagner basin; 3, Consag basin; 4, Delfin basin. The limit between PA (Pacific) and NA (North American) plates was defined from Lonsdale (1989) and Stock and Hodges (1989). The two arrows show the plate motion between both plates. BCP = Baja California Peninsula; GoC = Gulf of California.

sources and processes (e.g., mantle, organic matter, carbonate and carbide minerals, graphite, and diamonds; Clark & Fritz, 1997; Faure & Mensing, 2005; Sano & Marty, 1995).

In the Baja California Peninsula (BCP) and the Gulf of California (GoC), the degassing of volatiles is widespread and occurs within the geodynamic context of the cessation of the eastward subduction of the Farallon plate beneath the peninsula ~12 Ma ago (Atwater, 1970; Stock & Lee, 1994) and the formation and development of the rift in the GoC (Figure 1). The latter process has generated a high thermal gradient, which is associated with the thinning of the lithosphere and partial melting (Calmus et al., 2011). Further evidence of this rift is the presence of submarine hydrothermal manifestations at, e.g., the Guaymas basin, Pescadero basin, and Alarcon basin, where oceanic crust is being formed (Fenby & Gastil, 1991; Lonsdale, 1989) and high-temperature fluids (>240 °C) are discharged (Monterey Bay Aquarium Research Institute, 2012; Spelz et al., 2015; Von Damm et al., 1985). Associated with this regional process are numerous gas manifestations, mostly intertidal bubbling springs, and also submarine springs, fumaroles, and mud pools with temperatures between 30 and 100 °C, which are principally located within continental crust along the eastern coast of the BCP and almost parallel to the rift fracture (Figure 1). This degassing extends north to the Cerro Prieto and Salton Sea geothermal fields and to the

western coast of the peninsula. In the latter, the emission of gases is not related to the rifting process but to the presence of local faults (Polyak et al., 1982; Vidal et al., 1981).

Several investigations examined the geochemistry of volatiles that are emitted from the BCP. The studied gases are located in Punta Banda, Uruapan, Agua Caliente, San Carlos, San Valente, Valle de Guadalupe, San Antonio, Sierra Juárez, Puertecitos, Bahía Concepción, and El Chorro. Most of these studies focused on the characterization of the gas chemistry (Forrest et al., 2005; Vidal et al., 1981, 1982) and isotopic composition of light noble gases (Negrete-Aranda et al., 2015; Polyak et al., 1991; Vidal et al., 1981). In geothermal fields (e.g., the Salton Sea, Cerro Prieto, and Las Tres Vírgenes), noble gas and carbon isotopes have been the goal of multiple geochemical campaigns (Birkle et al., 2016; Des Marais et al., 1988; Galimov & Simoneit, 1982; Mazor & Truesdell, 1984; Mazzini et al., 2011; Pinti et al., 2018; Polyak et al., 1982; Richard et al., 2019; Truesdell et al., 1978; Welhan, 1981; Welhan et al., 1978). Other studies investigated submarine gases and fluid inclusions in minerals and/or rocks that are emitted from the spreading centers in the GoC (Castillo et al., 2002; Lupton, 1979; Spelz et al., 2015).

Data on light hydrocarbons are scarce and are mostly related to primary geothermal fields or submarine hydrothermal/sediment gases (e.g., Des Marais et al., 1988; Galimov & Simoneit, 1982; Mazzini et al., 2011; Welhan, 1981; Welhan & Lupton, 1987). The only reported data for the hydrothermal emissions from the BCP are from the Bahía Concepción (e.g., Forrest et al., 2005).

This work quantifies and elucidates for the first time the geochemistry of gas emissions that occurs along the eastern coast of the BCP. For these gases, we present chemical data and isotopic compositions of noble gases, CO<sub>2</sub>, and CH<sub>4</sub>. By integrating our data with existing data from the other BCP and GoC gas manifestations, we constrain the origin of these gases, identify the main processes that modify their pristine compositions, and evaluate the geotectonic implications. A comprehensive conceptual model to explain the nature of the gases that are emitted from the BCP is proposed to rationalize the relationship between the continental degassing of mantle-derived fluids and the lack of active volcanism.

## 2. Geodynamic and Volcano-Tectonic Setting

Continental rupture in the GoC began at ~5 Ma, when the East Pacific Rise (EPR) propagated northward and formed narrow extensional domains that are connected by transform faults, which progressively reached the northern gulf and the San Andreas fault system in the Salton basin. In the southernmost portion of the rift, the Alarcon basin has experienced seafloor spreading and the formation of oceanic crust with magnetic lineation since 3.5 Ma (Lonsdale, 1989). Further north, the Guaymas basin contains nearly 280 km of new oceanic crust under thick sedimentary deposits according to seismic refraction experiments, while the Delfin, Consag, and Wagner basins apparently have narrow troughs with oceanic crust under >6-km-thick sedimentary deposits from the Colorado River (González-Escobar et al., 2014; González-Fernández et al., 2005; Martín-Barajas et al., 2013; Persaud et al., 2003, Figure 1). These basins do not show obvious magnetic lineation (González-Fernández et al., 2005). On land, the amount of new crust in the Cerro Prieto basin following rift fracturing is still poorly constrained. This feature is more apparent in the Salton basin, which has a nearly ~100-km-long gap of continental crust under metamorphosed to lithified sedimentary rocks (Han et al., 2016).

Late Pliocene to Quaternary volcanic activity has occurred at several locations in the northern GoC and Salton trough, an axial rift valley that is 30-km long, half of which is overlapped by the Northern trough spreading center and is oblique to the spreading direction (Lonsdale & Becker, 1985). Recent volcanism has occurred at the intersection of transtensional fault domains and intervening dextral-slip transform faults. Felsic volcanism has been reported in the Salton Buttes (Robinson et al., 1976; Schmitt et al., 2013; Wright et al., 2015), Cerro Prieto (García-Sánchez et al., 2017; Schmitt et al., 2013), Roca Consag (Schmitt et al., 2013), and Delfin basins (Martín-Barajas et al., 2008). Mafic intrusive rocks and basaltic xenoliths have been found at the Cerro Prieto and Salton basin, indicating basaltic parent magma at depth (Herzig, 1990; Herzig & Elders, 1988; Schmitt et al., 2013).

In the San Luis Gonzaga region, Isla San Luis is the youngest known volcanic center in the northern GoC, whose last eruption occurred sometime after 4.7 ka ago (Hausback et al., 2003). Magmatic products from basaltic andesite to rhyolite indicate a complete magmatic evolution trend over a relatively short time interval (Paz-Moreno & Demant, 1999).

Toward the south, the Las Tres Virgenes Volcanic Zone (LTVVZ) has experienced diachronic volcanism since ~1.6 Ma in the La Reforma and Aguajito calderas (Garduño-Monroy et al., 1993). The Las Tres Virgenes volcanoes consist of La Virgen, El Azufre, and El Viejo and constitute the most recent volcanic activity in the LTVVZ. The first two have K/Ar ages of 44 and 28 ka, respectively (López et al., 1993, 1989). The eruption age of La Virgen is controversial, with reported ages of 6.5 ka (Capra et al., 1998) and 30 ka (Schmitt et al., 2010).

### 3. Sampling and Analytical Techniques

#### 3.1. Description of Sampling Sites

Between 2016 and 2017, thirty-two gas samples were collected from seven emissions along the eastern margin of the BCP (Figure 1 and Tables 1 and 2). Based on their respective location, we classify these gas manifestations as intertidal, subaerial, and submarine.

##### 3.1.1. Intertidal Gas Manifestations

Samples from intertidal sites were collected at San Felipe, Punta Estrella, Coloraditos, and Puertecitos (Figure 1). These emissions consist of bubbling gases that are associated with thermal waters. These sites are only accessible during low tide.

In San Felipe, over 200 springs are located in a 200-m-long and 30- to 60-m-wide area. Springs are located in both unconsolidated lithified sand and basement rocks that form rock cavities (Linn, 1978), with water temperatures between 35 and 49 °C.

The Punta Estrella thermal spring area is located approximately 15 km south of San Felipe. Here only two bubbling springs were sampled; the remaining manifestations were scarcely bubbling and difficult to observe. The average water temperature here is ~32 °C.

In Coloraditos, the hot springs are located on a layer of calcite-cemented fossiliferous volcanic lithoarenite, which forms a broad marine terrace. Consolidated Quaternary fluvial sandstone and gravel crop out above the sandy beach (Linn, 1978). The small springs, which are likely associated with NNW-SSE trending normal faults (Álvarez, 1995), are characterized by evaporation and a lack of gas exhalations (Barragán et al., 2001), reaching temperatures of 60 °C.

Puertecitos is a thermal spring that is located in small fractures within Late Pliocene welded ash-flow tuffs (Martín-Barajas et al., 1995). The spring manifests as occasional bubbling that ascends from the bottom of a natural intertidal pool with a water temperature up to 65 °C.

##### 3.1.2. Subaerial Gas Emissions

Subaerial gases were sampled at Agua Agria and at the Fumarole near the Las Tres Virgenes Geothermal Field (Figure 1). Agua Agria lies north of the El Aguajito caldera; hot springs and mud pools have temperatures from 50 to 99 °C. This zone is characterized by a small, intermittent stream.

The Fumarole is located approximately 5 km SSE of Agua Agria and consists of a prominent fumarole with abundant water vapor that reaches temperatures of nearly 100 °C.

##### 3.1.3. Submarine Gases

The San Luis Gonzaga region (Figure 1) includes six nearshore islands (e.g., El Huerfanito, El Muerto, El Coloradito, El Cholludo, Pómez, and San Luis). San Luis is the largest island (16 km<sup>2</sup>) and was formed by a series of Holocene explosive and effusive volcanism that began at 4.7 ka and continued to perhaps 1.2 ka according to <sup>14</sup>C dating ages from marine mollusk shells (Hausback et al., 2003). This island is characterized by a moderately rugged topography that was produced by two rhyolite domes, with its highest peak 220 m above sea level (Rossetter, 1970). The hydrothermal activity manifests as several submarine springs at depths of 10–15 m below sea level. Bubbles rise toward the sea surface on the NNE side of the island and between San Luis and Pómez.

#### 3.2. Sampling Techniques

Intertidal gases were sampled by using an overturned stainless steel funnel that was submerged in the water. This funnel was connected to a three-way valve and syringe to purge the flask and pressurize the gas during storage.

**Table 1**  
*Chemical Composition of the Dry Gases That Were Sampled in This Study*

Sample	Site	Type	Storage	Sampling date	N	E	pH	T (°C)	He (ppmV)	H <sub>2</sub> (ppmV)	O <sub>2</sub> (Vol.%)	N <sub>2</sub> (Vol.%)	CH <sub>4</sub> (Vol.%)	CO (ppmV)	CO <sub>2</sub> (Vol.%)	H <sub>2</sub> S (ppmV)	<sup>40</sup> Ar (ppmV)	<sup>36</sup> Ar (ppmV)	C <sub>2</sub> H <sub>6</sub> (ppmV)	C <sub>3</sub> H <sub>8</sub> (ppmV)
SF-1	San Felipe	Intertidal gas manifestations	Exetainer® glass vial	5/5/2016	31.0276	-114.8274	6.34	35.8	1.2	b.d.I	0.53	2.0	0.02	3.4	97.5	b.d.I	386.9	1.2	b.d.I	b.d.I
SF-2	San Felipe	Intertidal gas manifestations	Exetainer® glass vial	5/5/2016	31.0275	-114.8274	5.81	45.7	1.6	b.d.I	0.32	1.6	0.02	3.0	98.0	b.d.I	389.2	1.2	b.d.I	b.d.I
SF-3	San Felipe	Intertidal gas manifestations	Exetainer® glass vial	5/5/2016	31.0271	-114.8276	5.77	46.0	1.3	19.0	0.42	2.2	0.01	25.0	97.3	b.d.I	329.3	1.1	b.d.I	b.d.I
SF-4	San Felipe	Intertidal gas manifestations	Exetainer® glass vial	8/17/2016	31.0263	-114.8280	5.78	42.7	2.6	b.d.I	0.26	1.1	0.02	2.3	98.6	b.d.I	226.0	0.8	b.d.I	b.d.I
SF-5	San Felipe	Intertidal gas manifestations	Exetainer® glass vial	8/17/2016	31.0263	-114.8280	5.63	40.8	1.8	b.d.I	0.60	2.4	0.02	4.2	97.0	b.d.I	140.6	0.5	b.d.I	b.d.I
SF1 (SSB)	San Felipe	Intertidal gas manifestations	Stainless	2/26/2017	31.0276	-114.8274	5.60	42.0	b.d.I	b.d.I	0.04	1.1	0.01	b.d.I	98.9	b.d.I	273.8	0.9	b.d.I	b.d.I
SF2 (SSB)	San Felipe	Intertidal gas manifestations	Steel Bottle	2/26/2017	31.0275	-114.8274	6.31	40.2	b.d.I	b.d.I	0.04	0.4	0.01	b.d.I	99.6	b.d.I	95.7	0.3	b.d.I	b.d.I
PE-1	Punta Estrella	Intertidal gas manifestations	Steel Bottle	5/6/2016	30.9444	-114.7329	5.86	29.2	176.7	4.7	0.72	19.9	37.12	1.7	41.9	b.d.I	3605.1	12.2	169.7	b.d.I
PE-2	Punta Estrella	Intertidal gas manifestations	Exetainer® glass vial	5/6/2016	30.9445	-114.7329	5.86	30.1	93.1	4.1	0.76	12.2	28.72	3.1	58.1	b.d.I	2154.4	7.2	120.1	b.d.I
PE1 (SSB)	Punta Estrella	Intertidal gas manifestations	Stainless	2/26/2017	30.9444	-114.7329	5.86	29.2	68.2	4.6	0.06	7.5	22.76	b.d.I	69.5	b.d.I	1851.7	6.1	b.d.I	b.d.I
CO1y	Coloraditos	Intertidal gas manifestations	Steel Bottle	5/7/2016	30.5795	-114.6641	8.02	61.0	166.5	7.0	11.89	82.2	4.40	0.9	0.2	b.d.I	9538.5	32.2	278.8	b.d.I
CO2	Coloraditos	Intertidal gas manifestations	Exetainer® glass vial	5/7/2016	30.5797	-114.6638	8.10	55.2	378.6	7.0	2.69	88.0	8.04	0.6	0.2	b.d.I	10529.4	34.9	393.6	b.d.I
CO3	Coloraditos	Intertidal gas manifestations	Exetainer® glass vial	8/19/2016	30.5798	-114.6637	8.01	53.5	376.5	5.1	0.00	96.9	1.79	0.2	0.2	b.d.I	9680.9	32.4	b.d.I	b.d.I
PU1	Puertecitos	Intertidal gas manifestations	Exetainer® glass vial	11/16/2016	30.3461	-114.6360	6.67	57.2	200.3	8.9	0.08	72.5	11.05	4.9	15.5	1677.3	12215.4	40.3	3847.9	b.d.I
PU1 new	Puertecitos	Intertidal gas manifestations	Exetainer® glass vial	2/27/2017	30.3461	-114.6360	6.60	57.0	211.7	b.d.I	0.23	71.6	12.07	b.d.I	15.1	1385.1	3957.5	3923.0	3957.5	b.d.I
SLG1	San Luis Gonzaga	Submarine gases	Exetainer® glass vial	3/1/2017	29.9888	-114.4011	"."	"."	72.7	1.9	0.16	5.1	39.02	1.5	52.8	22209.7	1650.4	5.6	4542.9	129.2
SLG2	San Luis Gonzaga	Submarine gases	Exetainer® glass vial	3/1/2017	29.9874	-114.3981	"."	"."	118.4	1.5	0.05	7.6	39.75	1.7	49.3	24789.4	700.2	1.4	6475.6	171.0
SLG1 (SSB)	San Luis Gonzaga	Submarine gases	Stainless	3/1/2017	29.9888	-114.4011	"."	"."	213.2	b.d.I	0.17	19.6	64.33	b.d.I	14.3	b.d.I	3339.1	11.2	9439.6	249.7
SLG2 (SSB)	San Luis Gonzaga	Submarine gases	Steel Bottle	3/1/2017	29.9874	-114.3981	"."	"."	103.5	5357.2	0.04	10.9	50.62	6.1	36.0	8706.7	1583.9	5.3	5326.5	169.0
AA1	Agua Agria	Subaerial gas emissions	Steel Bottle	11/9/2016	27.5615	-112.5862	3.19	97.6	14.1	6063.7	0.67	3.7	0.25	10.0	94.2	4720.8	889.2	2.2	b.d.I	b.d.I
AA4	Agua Agria	Subaerial gas emissions	Exetainer® glass vial	11/10/2016	27.5615	-112.5862	3.31	65.3	15.0	6525.1	0.46	3.6	0.25	9.0	94.6	2806.5	650.0	2.2	b.d.I	b.d.I
AA5	Agua Agria	Subaerial gas emissions	Exetainer® glass vial	11/10/2016	27.5615	-112.5862	3.20	96.2	18.1	7393.9	2.47	12.6	0.26	14.1	83.8	b.d.I	420.1	1.4	b.d.I	b.d.I
AA7	Agua Agria	Subaerial gas emissions	Exetainer® glass vial	11/10/2016	27.5615	-112.5862	3.03	79.7	13.2	5979.1	0.11	3.3	0.23	15.2	95.7	b.d.I	537.5	1.8	b.d.I	b.d.I
AA4 (SSB)	Agua Agria	Subaerial gas emissions	Stainless	3/2/2017	27.5615	-112.5862	3.20	65.0	12.7	5756.1	0.02	2.6	0.21	3.7	96.2	4108.7	346.2	1.2	b.d.I	b.d.I
AA5 (SSB)	Agua Agria	Subaerial gas emissions	Steel Bottle	3/2/2017	27.5615	-112.5862	3.20	96.2	12.4	23367.5	0.01	2.6	0.22	3.5	94.2	5352.9	346.2	0.5	b.d.I	b.d.I
AA5 (SSB)	Agua Agria	Subaerial gas emissions	Steel Bottle	3/2/2017	27.5615	-112.5862	3.20	96.2	12.5	22026.0	0.04	2.8	0.21	5.0	94.4	1983.4	338.2	0.5	b.d.I	b.d.I
AA7 (SSB)	Agua Agria	Subaerial gas emissions	Stainless	3/2/2017	27.5615	-112.5862	3.03	79.7	11.3	5139.2	3.45	20.2	0.18	19.5	74.8	b.d.I	2362.0	0.0	b.d.I	b.d.I
FUM (SSB)	Tres Virgenes	Subaerial gas emissions	Steel Bottle	3/2/2017	27.5265	-112.5616	"."	97.0	7.0	3276.7	0.08	46.1	0.08	b.d.I	53.0	1293.9	5464.5	0.0	b.d.I	b.d.I

Note. b.d.I. means below detection limits; " ." means no data.  
<sup>a</sup>Indicates a replicate measurement of the same sample.

**Table 2**  
*Isotopic Composition of the Dry Gases That Were Sampled in This Study*

Sample	Site	Type	Storage	Sampling date	N	E	pH	T (°C)	R/Ra	He/Ne
SF-1	San Felipe	Intertidal gas manifestations	Exetainer® glass vial	5/5/2016	31.0276	-114.8274	6.34	35.8	1.09	2.40
SF-2	San Felipe	Intertidal gas manifestations	Exetainer® glass vial	5/5/2016	31.0275	-114.8274	5.81	45.7	1.07	2.77
SF-3	San Felipe	Intertidal gas manifestations	Exetainer® glass vial	5/5/2016	31.0271	-114.8276	5.77	46.0	1.09	2.07
SF-4	San Felipe	Intertidal gas manifestations	Exetainer® glass vial	8/17/2016	31.0263	-114.8280	5.78	42.7	1.11	3.36
SF-5	San Felipe	Intertidal gas manifestations	Exetainer® glass vial	8/17/2016	31.0263	-114.8280	5.63	40.8	1.07	13.04
SF1 (SSB)	San Felipe	Intertidal gas manifestations	Stainless Steel Bottle	2/26/2017	31.0276	-114.8274	5.60	42.0	1.12	2.75
SF2 (SSB)	San Felipe	Intertidal gas manifestations	Stainless Steel Bottle	2/26/2017	31.0275	-114.8274	6.31	40.2	1.15	6.86
PE-1	Punta Estrella	Intertidal gas manifestations	Exetainer® glass vial	5/6/2016	30.9444	-114.7329	5.86	29.2	1.17	115.47
PE-2	Punta Estrella	Intertidal gas manifestations	Exetainer® glass vial	5/6/2016	30.9445	-114.7329	5.86	30.1	1.08	91.18
PE1 (SSB)	Punta Estrella	Intertidal gas manifestations	Stainless Steel Bottle	2/26/2017	30.9444	-114.7329	5.86	29.2	1.12	78.90
CO1y	Coloraditos	Intertidal gas manifestations	Exetainer® glass vial	5/7/2016	30.5795	-114.6641	8.02	61.0	0.81	17.28
CO2	Coloraditos	Intertidal gas manifestations	Exetainer® glass vial	5/7/2016	30.5797	-114.6638	8.10	55.2	1.07	35.77
CO3	Coloraditos	Intertidal gas manifestations	Exetainer® glass vial	8/19/2016	30.5798	-114.6637	8.01	53.5	0.58	2.03
PU	Puertecitos	Intertidal gas manifestations	Exetainer® glass vial	5/8/2016	30.3461	-114.6360	6.67	60.0	1.43	10.85
PU1	Puertecitos	Intertidal gas manifestations	Exetainer® glass vial	11/16/2016	30.3461	-114.6360	6.67	57.2	1.59	19.37
PU1 new	Puertecitos	Intertidal gas manifestations	Exetainer® glass vial	2/27/2017	30.3461	-114.6360	6.60	57.0	1.55	17.74
SLG1	San Luis Gonzaga	Submarine gases	Exetainer® glass vial	3/1/2017	29.9888	-114.4011	“.”	“.”	6.88	87.00
SLG2	San Luis Gonzaga	Submarine gases	Exetainer® glass vial	3/1/2017	29.9874	-114.3981	“.”	“.”	6.90	103.66
SLG1(SSB)	San Luis Gonzaga	Submarine gases	Stainless Steel Bottle	3/1/2017	29.9888	-114.4011	“.”	“.”	6.84	170.82
SLG2 (SSB)	San Luis Gonzaga	Submarine gases	Stainless Steel Bottle	3/1/2017	29.9874	-114.3981	“.”	“.”	6.88	125.19
AA1	Agua Agria	Subaerial gas emissions	Exetainer® glass vial	11/9/2016	27.5615	-112.5862	3.19	97.6	5.45	11.69
AA2	Agua Agria	Subaerial gas emissions	Exetainer® glass vial	11/9/2016	27.5615	-112.5862	3.31	65.3	5.10	2.97
AA3	Agua Agria	Subaerial gas emissions	Exetainer® glass vial	11/9/2016	27.5615	-112.5862	3.13	99.5	4.71	2.47
AA4	Agua Agria	Subaerial gas emissions	Exetainer® glass vial	11/10/2016	27.5615	-112.5862	3.31	65.3	5.54	19.97
AA5	Agua Agria	Subaerial gas emissions	Exetainer® glass vial	11/10/2016	27.5615	-112.5862	3.20	96.2	5.46	24.62
AA6	Agua Agria	Subaerial gas emissions	Exetainer® glass vial	11/10/2016	27.5615	-112.5862	3.51	96.2	4.63	2.48
AA7	Agua Agria	Subaerial gas emissions	Exetainer® glass vial	11/10/2016	27.5615	-112.5862	3.03	79.7	5.13	18.48
AA4 (SSB)	Agua Agria	Subaerial gas emissions	Stainless Steel Bottle	3/2/2017	27.5615	-112.5862	3.20	65.0	5.64	21.38
AA5 (SSB)	Agua Agria	Subaerial gas emissions	Stainless Steel Bottle	3/2/2017	27.5615	-112.5862	3.20	96.2	5.41	18.58
AA5 <sup>a</sup> (SSB)	Agua Agria	Subaerial gas emissions	Stainless Steel Bottle	3/2/2017	27.5615	-112.5862	3.20	96.2	5.43	21.64
AA7 (SSB)	Agua Agria	Subaerial gas emissions	Stainless Steel Bottle	3/2/2017	27.5615	-112.5862	3.03	79.7	5.06	2.14
FUM (SSB)	Tres Virgenes	Subaerial gas emissions	Stainless Steel Bottle	3/2/2017	27.5265	-112.5616	“.”	97.0	4.29	0.70

*Note.* The  $^3\text{He}/^4\text{He}$  ratios are expressed as R/Ra, where the  $^3\text{He}/^4\text{He}$  ratio in the sample (R) is normalized to the same ratio in the atmosphere (Ra =  $1.39 \cdot 10^{-6}$ ; Clarke et al., 1976; Mabry et al., 2013; Mamyrin et al., 1970; Sano et al., 2008). The Rc/Ra values represent the  $^3\text{He}/^4\text{He}$  ratio corrected for atmospheric contamination. The  $\delta^{13}\text{C}_{\text{CO}_2}$  and  $\delta^{13}\text{C}_{\text{CH}_4}$  values are reported in per mil relative to the VPDB standard. The  $\delta\text{D}_{\text{CH}_4}$  values are reported in per mil against the VSMOW standard. The isotope data for  $\text{CH}_4$  in San Felipe and Agua Agria are from Giggenbach bottles. The mantle contribution was calculated by using a binary model, with the  $^3\text{He}/^4\text{He}$  value of Alarcon lavas as the magmatic end-member ( $\sim 8.4 \pm 0.14$  Ra, Castillo et al., 2002). b.d.l. means below detection limits; “.” means no data. VPDB = Vienna Pee Dee Belemnite; VSMOW = Vienna Standard Mean Ocean Water.

<sup>a</sup>Indicates a replicate measurement of the same sample.

Subaerial gases from the LTVVZ were sampled by using a 50-cm-long stainless steel tube that was inserted into the soil. Further details on the sampling techniques can be found in Rizzo et al. (2015).

Submarine gases from San Luis Gonzaga were directly sampled at the sea bottom by a scuba diver, with the same technique for intertidal gases.

Two types of preevacuated bottles were used to store dry gases: (1) two-valve, stainless steel bottles; and (2) a single-valve, Giggenbach-like glass bottle. When gas flow was very low, we stored gases in Exetainer® screw-capped glass vials by using the water displacement technique. Each vial was placed in a plastic bottle that was filled with water to reduce the risk of air contamination. The chemistry and noble gas isotopes in the vials were analyzed after sampling, with replicate measurements conducted afterward to confirm the results.

An additional campaign of gas collection and storage in proper bottles confirmed the reliability of the results from the vials.

### 3.3. Analytical Techniques

Chemical and isotope analyses were conducted at the Istituto Nazionale di Geofisica e Vulcanologia, Sezione di Palermo, Italy (INGV-Palermo). The concentrations of He, H<sub>2</sub>, O<sub>2</sub>, N<sub>2</sub>, CH<sub>4</sub>, CO, H<sub>2</sub>S, C<sub>2</sub>H<sub>6</sub>,

Table 2 (continued)

Sample	<sup>3</sup> He (ppmV)	<sup>4</sup> He (ppmV)	<sup>20</sup> Ne (ppmV)	Rc/ Ra	Error (+/-)	<sup>40</sup> Ar (ppmV)	<sup>36</sup> Ar (ppmV)	<sup>40</sup> Ar/ <sup>36</sup> Ar	Error (+/-)	<sup>38</sup> Ar/ <sup>36</sup> Ar	Error (+/-)	δ <sup>13</sup> C(CO <sub>2</sub> ) (‰ vs VPDB)	δ <sup>13</sup> C(CH <sub>4</sub> ) (‰ vs VPDB)	δD(CH <sub>4</sub> ) (‰ vs. VSMOW)	Mantle contribution (%)
SF-1	1.93E-06	1.26	0.52	1.11	0.01	386.9	1.22	315	0.061	0.192	0.0001	-5.0	"-"	"-"	13.2
SF-2	2.17E-06	1.45	0.52	1.08	0.01	389.2	1.24	313	0.053	0.193	0.0001	-5.3	"-"	"-"	12.8
SF-3	1.94E-06	1.27	0.61	1.10	0.01	329.3	1.11	295	0.060	0.187	0.0002	-5.1	"-"	"-"	13.1
SF-4	1.92E-06	1.23	0.37	1.12	0.01	226.0	0.78	298	0.253	0.187	0.0002	-5.0	"-"	"-"	13.4
SF-5	2.11E-06	1.41	0.11	1.08	0.01	140.6	0.48	298	0.260	0.187	0.0002	-5.0	"-"	"-"	12.8
SF1 (SSB)	9.47E-07	0.60	0.22	1.14	0.01	273.8	0.94	295	0.071	0.187	0.0001	-5.0	23.1	317	13.6
SF2 (SSB)	1.29E-06	0.80	0.12	1.16	0.01	94.7	0.32	295	0.065	0.187	0.0002	-5.0	23.4	333	13.8
PE-1	2.78E-04	170.72	1.48	1.17	0.01	3605.1	12.19	296	0.091	0.188	0.0001	-6.6	-43.6	-168	14.0
PE-2	1.37E-04	91.69	1.01	1.08	0.01	2154.4	7.17	301	0.096	0.188	0.0002	-5.2	-40.1	-162	12.8
PE1 (SSB)	1.06E-04	67.93	0.86	1.12	0.01	1851.7	6.14	301	0.054	0.189	0.0001	-6.0	-39.3	-157	13.4
CO1y	1.92E-04	170.45	9.86	0.81	0.01	9538.5	32.22	297	0.073	0.188	0.0001	-17.7	1.1	146	9.6
CO2	4.75E-04	317.92	8.89	1.08	0.01	10529.4	34.93	302	0.074	0.188	0.0001	-18.4	3.4	137	12.8
CO3	2.25E-05	32.34	15.94	0.50	0.02	9680.9	32.42	298	0.076	0.187	0.0001	-18.1	"-"	"-"	6.0
PU	2.92E-04	145.69	13.42	1.44	0.02	3379.7	11.37	298	0.079	0.191	0.0001	-11.7	38.1	"-"	17.2
PU1	4.49E-04	201.67	10.41	1.60	0.02	12215.4	40.29	303	0.082	0.191	0.0001	-11.0	13.5	"-"	19.1
PU1 new	4.55E-04	210.21	11.85	1.56	0.02	11678.5	39.23	298	0.060	0.189	0.0004	-9.9	12.4	"-"	18.5
SLG1	1.82E-03	189.59	2.18	6.90	0.06	1650.4	5.57	297	0.079	0.186	0.0002	-10.5	-26.8	-70	82.2
SLG2	9.94E-04	103.34	1.00	6.92	0.06	700.2	2.35	300	0.099	0.187	0.0002	-10.9	-27.4	-100	82.4
SLG1(SSB)	1.26E-03	132.05	0.77	6.86	0.06	3339.1	11.23	298	0.111	0.189	0.0003	-9.6	-24.6	-76	81.6
SLG2 (SSB)	6.97E-04	72.81	0.58	6.89	0.06	1583.9	5.25	303	0.090	0.188	0.0002	-11.3	-27.2	-97	82.0
AA1	1.11E-04	14.31	1.22	5.57	0.05	889.2	2.98	298	0.114	0.191	0.0002	-10.7	"-"	"-"	66.3
AA2	1.09E-04	14.07	4.73	5.59	0.05	1936.2	6.36	304	0.105	0.191	0.0001	-11.1	"-"	"-"	66.6
AA3	9.86E-05	13.50	5.47	5.26	0.04	3579.3	11.89	301	0.057	0.191	0.0001	-10.6	"-"	"-"	62.6
AA4	1.24E-04	15.91	0.80	5.62	0.04	650.0	2.17	300	0.099	0.192	0.0003	-10.3	"-"	"-"	66.9
AA5	1.07E-04	13.99	0.57	5.52	0.04	420.1	1.41	298	0.191	0.191	0.0006	-9.8	"-"	"-"	65.7
AA6	9.04E-05	12.59	5.08	5.17	0.04	3228.8	10.76	300	0.055	0.190	0.0001	-10.2	"-"	"-"	61.5
AA7	1.00E-04	13.83	0.75	5.20	0.04	537.5	1.80	299	0.154	0.191	0.0005	"-"	"-"	"-"	62.0
AA4 (SSB)	9.67E-05	12.17	0.57	5.71	0.04	346.2	1.17	297	0.081	0.188	0.0002	"-"	-30.0	-105	68.0
AA5 (SSB)	9.60E-05	12.58	0.68	5.49	0.05	346.2	1.2	297	0.081	0.188	0.0002	"-"	"-"	"-"	65.4
AA5 (SSB)	9.78E-05	12.79	0.59	5.50	0.05	338.2	1.1	297	0.091	0.188	0.0002	"-"	"-"	"-"	65.5
AA7 (SSB)	9.53E-05	11.88	5.56	5.77	0.04	2361.6	7.9	298	0.063	0.188	0.0001	"-"	-30.3	-119	68.7
FUM (SSB)	6.94E-05	7.09	10.17	7.04	0.05	5464.5	18.4	297	0.071	0.189	0.0002	-10.5	"-"	"-"	83.8

C<sub>3</sub>H<sub>8</sub>, and CO<sub>2</sub> were determined by gas chromatography, following the methodology in Rizzo et al. (2015, 2016).

The isotopic analyses (<sup>13</sup>C/<sup>12</sup>C of CO<sub>2</sub>, <sup>13</sup>C/<sup>12</sup>C and D/H of CH<sub>4</sub>) were performed using a Delta Plus XP IRMS (Isotope Ratio Mass Spectrometry) that was equipped with a Thermo TRACE GC interfaced with Thermo GC/C III (for carbon) and Thermo GC/TC (for hydrogen). The Thermo TRACE gas chromatograph was equipped with a Poraplot-Q column (30 m × 0.32 mm i.d.), and the oven was held at a constant temperature (50 °C for carbon and 40 °C for hydrogen). The flow rate of the carrier gas (He of 5.6 grade) was kept at a constant flux of 0.8 cc/min. The injection system, which was described in more detail by Grassa et al. (2010), consists of a split/splitless injector with a split ratio from 10:1 to 80:1. Direct on-column injection was performed for diluted samples with a CO<sub>2</sub> and/or CH<sub>4</sub> concentration < 0.1 mmol/mol.

CH<sub>4</sub> was quantitatively converted to CO<sub>2</sub> by passing through a combustion oven (T = 940 °C) or H<sub>2</sub> by passing through a reactor set at a temperature of 1440 °C. The <sup>13</sup>C/<sup>12</sup>C ratios are reported as δ<sup>13</sup>C values against the Vienna Pee Dee Belemnite standard, and the <sup>2</sup>H/<sup>1</sup>H ratios are reported as δD values against the Vienna Standard Mean Ocean Water standard. The external analytical precision (1σ) is better than 0.1‰ for the <sup>13</sup>C/<sup>12</sup>C ratios (both CO<sub>2</sub> and CH<sub>4</sub>) and 1‰ for the D/H ratios, as computed through 10 repeated analyses of the same sample.

The elemental and isotope compositions of He (<sup>3</sup>He/<sup>4</sup>He) and <sup>20</sup>Ne were determined on the dry-gas samples by using a Helix SFT-GVI and Helix MC-Plus (Thermo Scientific) mass spectrometer for He and Ne, respectively, with <1.5% analytical error. The Ar concentration and isotope ratios (<sup>40</sup>Ar/<sup>36</sup>Ar) were measured in a

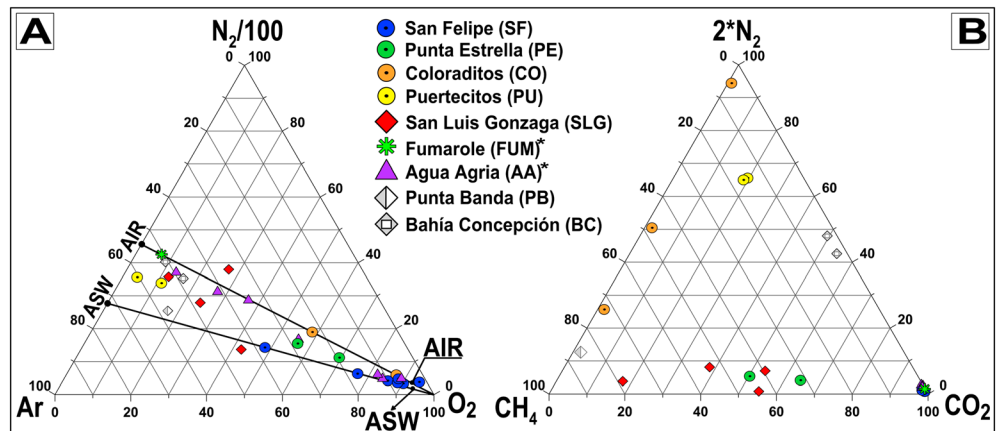


**Figure 2.** (a) Triangular  $N_2$ -Ar- $O_2$  plot from uncorrected chemical data to show the atmospheric contamination. The points air and ASW (*air saturated water*) on the  $N_2$ /Ar line were established from Giggenbach (1992). (b) Triangular  $N_2$ - $CH_4$ - $CO_2$  plot that was proposed by Giggenbach (1992), in which only data that were corrected for air contamination were plotted. More details on the air-correction procedure are reported in Table S1. The colored symbols correspond to the gas emissions that were sampled in this study, while those in gray relate to data produced in previous studies. In both plots, the data for PB and BC were taken from Vidal et al. (1981) and Forrest et al. (2005), respectively.

multicollector mass spectrometer (Helix MC-GVI), for which the analytical uncertainty was generally  $<0.5\%$ . Further details on the method and analytical errors can be found in Rizzo et al. (2015, 2016). The data are reported as R/Ra units (Ra is the  $^3\text{He}/^4\text{He}$  atmospheric ratio:  $1.39 \cdot 10^{-6}$ ; Clarke et al., 1976; Mamyrin et al., 1970).

## 4. Results

### 4.1. Gas Composition

The collected gases showed highly variable chemical composition (Tables 1 and S1 in the supporting information). In the  $N_2$ -Ar- $O_2$  triangular plot, almost all the samples showed  $N_2$ /Ar ratios between air and air saturated water at 25 °C (Figure 2a), suggesting that the  $N_2$  and Ar contributions were mainly atmospheric rather than originating from a deep source. The scattering of the data was related to a variable  $O_2$  content, which was caused by different extents of oxygen consumption because  $O_2$  is involved in many redox reactions. The atmospheric contamination could be intrinsic, that is, before gas collection or it may occur during the sampling and/or sample storage.

Therefore, we corrected the data from the atmospheric contribution by using the  $^{36}\text{Ar}$  contents (see Table S1 for more details), assuming that all the  $^{36}\text{Ar}$  was atmospheric in origin (e.g., Correale et al., 2016). We chose this approach because correction through  $O_2$  contents may underestimate the air contribution when oxygen is consumed during redox reactions, inducing appreciable changes in the final concentration of species. Hereafter, the air-corrected gas composition is used for data interpretation.

As shown in Figure 2b, the chemistry of the gases significantly varied among the sites. We distinguished three main groups: (1)  $CO_2$  dominated, which includes San Felipe, Punta Estrella, Agua Agria, and the Fumarole, with  $CO_2$  concentrations from 51.5 to almost 100%; (2)  $N_2$  dominated, which includes Puertecitos and one sample from Coloraditos, with an  $N_2$  content between 47.8 and 89.5%; and (3)  $CH_4$  dominated, including the two remaining Coloraditos samples with  $CH_4$  contents up to 82%. The San Luis Gonzaga samples showed variable composition, with one sample being  $CO_2$  dominated and the other two samples being  $CH_4$  dominated.

Ethane was present at levels of thousands of parts per million (ppm) at San Luis Gonzaga, Puertecitos, and Coloraditos and hundreds of ppm at Punta Estrella, while the values were below the detection limit (1 ppm) at San Felipe, Agua Agria, and the Fumarole (Table S1). Propane was only detected at San Luis Gonzaga and measured 136–300 ppm (Table S1). The Bernard parameter, which is expressed as  $C_1/(C_2 + C_3)$  (i.e.,



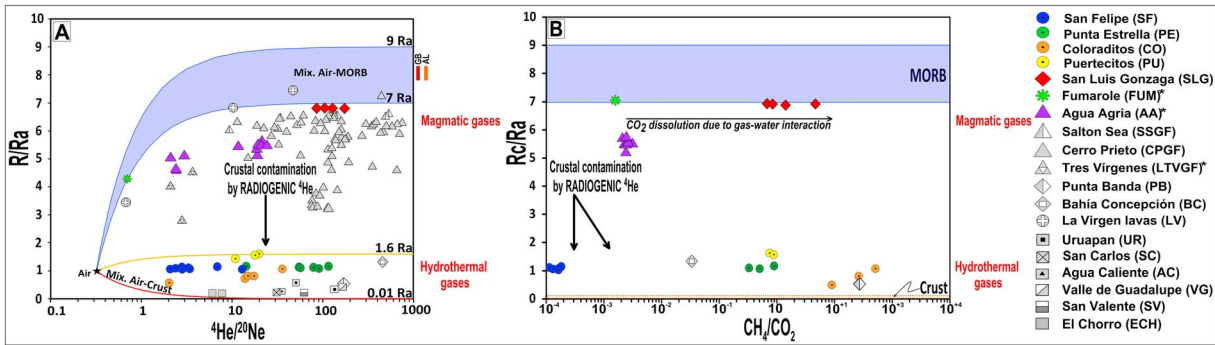


**Figure 3.** (a)  $R/Ra$  versus  ${}^4\text{He}/{}^{20}\text{Ne}$  plot. We report three paths of binary mixing between AIR ( ${}^4\text{He}/{}^{20}\text{Ne} = 0.318$ ,  $R/Ra = 1$ ), CRUST ( ${}^4\text{He}/{}^{20}\text{Ne} = 1000$ ,  $R/Ra = 0.01$ ), and MORB ( ${}^4\text{He}/{}^{20}\text{Ne} = 1000$ ,  $R/Ra = 7-9$ ; Sano & Wakita, 1985), alongside a local hydrothermal term (Puertecitos,  ${}^4\text{He}/{}^{20}\text{Ne} = 1000$  and  $R/Ra = 1.6$ ). AL indicates  ${}^3\text{He}/{}^4\text{He}$  data for fluid inclusions from Alarcón lavas (Castillo et al., 2002), while GB indicates data from Guaymas basin submarine gases (Lupton, 1979). In both sites,  ${}^4\text{He}/{}^{20}\text{Ne}$  was assumed  $>1,000$ . The distinction between colored and gray symbols is as in Figure 2 caption. The reported literature data are as follows: SSGF from Mazzini et al. (2011); CPGF from Welhan et al. (1978), Polyak et al. (1982), Birkle et al. (2016), and Pinti et al. (2018); LTVGF from Birkle et al. (2016); LV from Schmitt et al. (2010); PB, SC, and UR from Vidal et al. (1981); UR, AC, SC, SV, VG, SA, and ECH from Polyak et al. (1991); and BC from Forrest et al. (2005). (b) Binary plot of the  $\text{CH}_4/\text{CO}_2$  ratio versus  ${}^3\text{He}/{}^4\text{He}$  corrected for air contamination ( $Rc/Ra$ ). The fields MORB and CRUST were established from Graham (2002) and Morrison and Pine (1955), respectively.

methane/(ethane + propane); Bernard et al., 1978) was around 2,300 at Punta Estrella, between 157 and 204 at Coloraditos, and below 100 at Puertecitos and San Luis Gonzaga.

## 4.2. Isotope Composition

### 4.2.1. Noble Gases

The concentrations of He, Ne, and Ar and their isotopic compositions ( ${}^3\text{He}/{}^4\text{He}$  and  ${}^{40}\text{Ar}/{}^{36}\text{Ar}$ ) in the sampled gases are shown in Tables 1, 2, and S1 respectively.

The contents of helium were extremely variable, ranging from 1.1 ppm at San Felipe to more than 3,800 ppm at Coloraditos and showing an inverse relationship with  $\text{CO}_2$ . Samples with  $\text{CO}_2 > 90\%$  had the lowest He content ( $<15$  ppm), while those  $\text{N}_2$  and  $\text{CH}_4$  dominated (and consequently low  $\text{CO}_2$ ) displayed the highest He content (up to 3,800 ppm).

The  ${}^3\text{He}/{}^4\text{He}$  ratios also showed a wide variability, ranging between 0.6 and 6.9 Ra (Figure 3a). The highest values were measured at San Luis Gonzaga, whereas Agua Agria (4.6–5.6 Ra) and the Fumarole (4.3 Ra) had slightly lower ratios (Table 2). Previous studies in production wells in Las Tres Vírgenes geothermal field, which is near to the Fumarole and Agua Agria, revealed  ${}^3\text{He}/{}^4\text{He}$  values of 1–4.5 Ra (Birkle et al., 2016), which are lower than our findings. Notably, Agua Agria, Fumarole, and San Luis Gonzaga showed chemical variability (e.g.,  $\text{CH}_4/\text{CO}_2$ ) at almost constant  ${}^3\text{He}/{}^4\text{He}$  ratios (Figure 3b).

The gases from San Felipe and Punta Estrella varied within a narrow range (1.1–1.2 Ra). Otherwise, Puertecitos showed 1.4–1.6 Ra (Figure 3a), which is comparable to previous measurements (1.7 Ra) by Negrete-Aranda et al. (2015). Coloraditos showed variable  ${}^3\text{He}/{}^4\text{He}$  values between 0.6 and 1.1 Ra and is the only gas emission site along the eastern coast of the BCP with helium isotope ratios  $<1.1$  Ra (Table 2 and Figure 3a). In addition, these gases show a wide chemical variability (e.g.,  $\text{CH}_4/\text{CO}_2$ ) compared to the much smaller range of  ${}^3\text{He}/{}^4\text{He}$  ratios (Figure 3b).

The  ${}^4\text{He}/{}^{20}\text{Ne}$  ratio of the sampled gases varied from 0.7 (Fumarole) to 170 (San Luis Gonzaga), suggesting variable contamination by the atmosphere ( ${}^4\text{He}/{}^{20}\text{Ne} = 0.318$ ; e.g., Sano & Wakita, 1985), as already indicated by the chemistry (see section 4.1). However, this ratio usually exceeded that of air by tens to hundreds of times, leading to minor or negligible modifications of the pristine  ${}^3\text{He}/{}^4\text{He}$  (Figure 3a). Nonetheless, the  ${}^3\text{He}/{}^4\text{He}$  ratios were corrected for air contamination based on the measured  ${}^4\text{He}/{}^{20}\text{Ne}$  ratio (Sano et al., 2006) as follows:

$$R/Ra = ((R_M/Ra)(\text{He}/\text{Ne})_M - (\text{He}/\text{Ne})_A) / ((\text{He}/\text{Ne})_M - (\text{He}/\text{Ne})_A)$$

where the subscripts M and A refer to the measured and atmosphere theoretical values, respectively ( $\text{He}/\text{Ne}$ )<sub>A</sub> = 0.318). The corrected  ${}^3\text{He}/{}^4\text{He}$  ratios are hereafter reported as  $Rc/Ra$ . Only in FUM, which has a larger

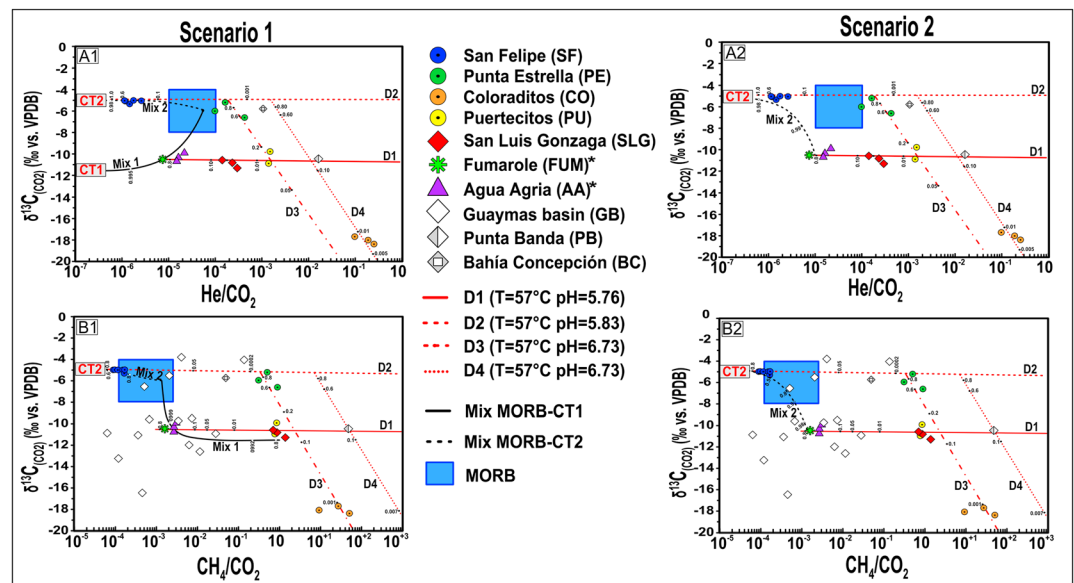


**Figure 4.** Binary plots of  $\delta^{13}\text{C}_{\text{CO}_2}$  versus  $\text{He}/\text{CO}_2$  (4a1 and 4a2) and  $\text{CH}_4/\text{CO}_2$  (4b1 and 4b2). Plots 4a1 and 4b1 refer to interpretative scenario 1, while 4a2 and 4b2 to scenario 2 (see text for details). In both plots, the  $\delta^{13}\text{C}_{\text{CO}_2}$  range for MORB is from Pineau and Javoy (1983), Javoy et al. (1986), and Marty and Jambon (1987). The  $\text{He}/\text{CO}_2$  range for MORB was taken from Jambon et al. (1985), Charlou and Donval (1993), and Trull et al. (1993). The  $\text{CH}_4/\text{CO}_2$  range for MORB was established from Jambon et al. (1985) and Charlou and Donval (1993). The  $\text{CH}_4/{}^3\text{He}$  data from MORB and crust/sediments were used to calculate the Mix 2 (Figures 4b1 and 4b2). The  $\text{CH}_4/{}^3\text{He}$  ratio in MORB was established from Merlivat et al. (1987), Welhan and Craig (1982), and Welhan and Craig (1983), while the  $\text{CH}_4/{}^3\text{He}$  ratio for crust/sediment data was taken from Wen et al. (2016). In both cases, the data are the averages. Mix 1 (black solid curve) and Mix 2 (black dotted curve) represent two binary mixing paths between MORB and two crustal end-members with different  $\delta^{13}\text{C}_{\text{CO}_2}$  values of  $-11\text{‰}$  and  $-5\text{‰}$  for CT1 and CT2, respectively. D1, D2, D3, and D4 are the paths of Rayleigh distillation modeling for the partial dissolution of  $\text{CO}_2$  in water at variable temperature and pH conditions (indicated in the legend), as assumed from gas emission conditions (when available) or assumed to fit data. See the text for details. The distinction between colored and gray symbols is as in Figure 1 caption.

atmospheric contribution ( ${}^4\text{He}/{}^{20}\text{Ne} = 0.7$ ), does this correction probably overestimate  ${}^3\text{He}/{}^4\text{He}$  (7.0 Ra; Figures 3a and 3b).

The  ${}^{40}\text{Ar}/{}^{36}\text{Ar}$  ratio fell within a narrow range (295–315) close to the theoretical ratio in the atmosphere (295.5; Ozima & Podosek, 1983), confirming the variable extent of air contamination. For this reason,  ${}^{40}\text{Ar}$  was not corrected ( ${}^{40}\text{Ar}^*$ ) and is not discussed further.

#### 4.2.2. $\text{CO}_2$ and $\text{CH}_4$

$\text{CO}_2$  and  $\text{CH}_4$  were analyzed for their isotope composition, and the data are reported in Table 2. The  $\delta^{13}\text{C}_{\text{CO}_2}$  values ranged from around  $-5.0\text{‰}$  at San Felipe and Punta Estrella to  $-18.4\text{‰}$  at Coloraditos (Figures 4a1, 4b1 and 4A2, 4b2), without any systematic correlation with  $\text{CO}_2$  concentration.

The carbon and hydrogen isotopes of  $\text{CH}_4$  showed a wide range of compositions from negative values toward unusually positive values (Figures 5a and 5b). The lowest  $\delta^{13}\text{C}_{\text{CH}_4}$  values were observed in Punta Estrella ( $\delta^{13}\text{C}_{\text{CH}_4}$  from  $-39.3$  to  $-43.6\text{‰}$  and  $\delta\text{D}_{\text{CH}_4} = -168\text{‰}$ ) and Agua Agria ( $\delta^{13}\text{C}_{\text{CH}_4}$  around  $-30\text{‰}$  and  $\delta\text{D}_{\text{CH}_4}$  from  $-119$  to  $-105\text{‰}$ ).

No spatial variations in the  $\text{CO}_2$  or  $\text{CH}_4$  isotope composition were observed.

## 5. Discussion

### 5.1. Origin of Gases in the BCP

#### 5.1.1. ${}^3\text{He}/{}^4\text{He}$ Signature

To constrain the origin of gases, we considered the chemistry and isotopic composition of He,  $\text{CO}_2$ , and  $\text{CH}_4$ . Based on the  ${}^3\text{He}/{}^4\text{He}$  ratios, we subdivided the collected samples in two groups: (1) magmatic and (2) hydrothermal gases (Figures 3a and 3b).

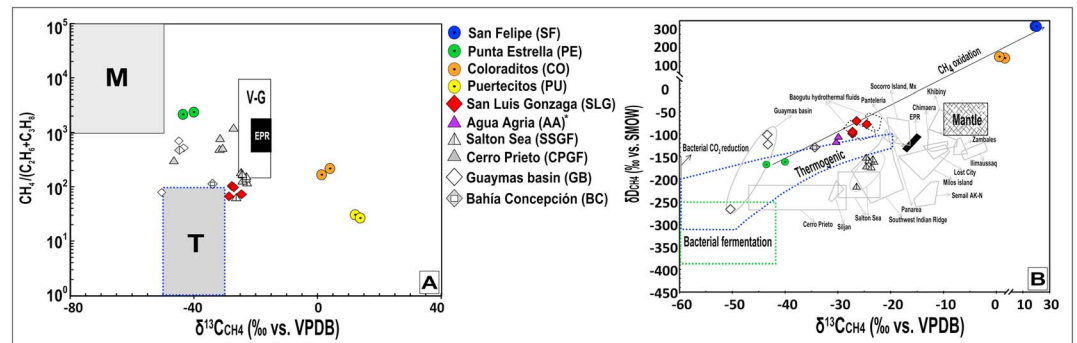


**Figure 5.** Origin of hydrocarbons in gas emissions along the eastern BCP. (a) Bernard diagram modified from Bernard et al. (1978). In the plot: M, microbial source from Schoell (1988) and Whiticar (1999); T, thermogenic source from Whiticar (1999); and V-G, volcanic-geothermal fields as defined by McCollom and Seewald (2007). (b) CD diagrams modified from Schoell (1983). In the plot, bacterial CO<sub>2</sub> reduction, bacterial fermentation, and thermogenic fields were established from Schoell (1988). Mantle field and isotopic data from the Baogutu hydrothermal fluids were taken from Cao et al. (2014). The polygonal gray fields and the small black triangle (i.e., Panteleria) were edited from Etiope and Sherwood-Lollar (2013). The other gray polygons are as follows: Cerro Prieto from Des Marais et al. (1988) and Welhan and Lupton (1987); Salton Sea fields from Welhan and Lupton (1987), Welhan (1988), and Mazzini et al. (2011); and Guaymas circular field from Welhan (1988). In both diagrams, the East Pacific Rise (EPR) field was defined from Welhan and Craig (1983). The distinction between colored and gray symbols is as in Figure 1 caption. The X and Y axes are broken to graph positive values. The black arrow shows changes in the isotope composition because of methane oxidation. See the text for further details. BCP = Baja California Peninsula.

1. Magmatic gases include gas emissions in areas of Quaternary to Holocene volcanic activity (e.g., San Luis Gonzaga, Agua Agria, and Fumarole). For these sites, a clear and strong magmatic signature, with  $^3He/^4He$  ratios of  $\sim 5\text{--}7$  Ra is found (Figure 6a1 and 6a2). Despite these volcanoes' location, these  $^3He/^4He$  values are slightly lower than the typical MORB range ( $8 \pm 1$  Ra; Graham, 2002).

This group also includes other gas emissions (Salton Sea and Cerro Prieto geothermal fields; Figures 1 and 3a) in the northeastern BCP. Gases from Salton Sea have  $^3He/^4He$  ratios of 6.1–6.6 Ra (Mazzini et al., 2011), while those from Cerro Prieto are in the range 3.3–7.3 Ra (Pinti et al., 2018; Polyak et al., 1982; Welhan et al., 1978). This magmatic signature is associated with volcanic activity that occurred less than 25 ka ago (Schmitt et al., 2012, 2013). The variability of the  $^3He/^4He$  ratios in Cerro Prieto Geothermal field indicates variable crustal contamination by radiogenic  $^4He$  produced at a local scale from U-Th-rich country rocks (Mazor & Truesdell, 1984; Welhan et al., 1978). A recent and detailed study carried out by Pinti et al. (2018) points to limited modern freshwater recharge and thus to the presence of a nearly fossil geothermal system. In detail, the authors suggest that connate waters dominate the central portion of the field and mix with the magmatic fluid containing mantle He that enter laterally into the reservoir, through the main lateral strike-slip faults (i.e., the Cerro Prieto and Imperial faults).

On the other hand, the measured  $^3He/^4He$  ratios in fluid inclusions of olivine crystals from mafic lavas that were sampled at La Virgen volcano revealed values of  $7.3 \pm 0.6$  Ra (Schmitt et al., 2010), which are at the lower limit of the typical MORB range. A slightly higher  $^3He/^4He$  ratio was present in submarine gases and volcanic rocks along the rift in the GoC (Figures 1 and 3a). In detail, fluids from Guaymas basin, Pescadero basin, and Alarcón basin yielded  $^3He/^4He$  ratios of  $\sim 8.0$  (Lupton, 1979),  $\sim 7.9$ , and 8.2 Ra, respectively (Spelz et al., 2015), while fluid inclusions in Alarcón basin basalt glasses yielded  $^3He/^4He$  ratios of 7.7–8.4 Ra (Castillo et al., 2002).

2. Hydrothermal gases (e.g., San Felipe, Punta Estrella, Coloraditos, and Puertecitos) are emitted mainly as intertidal gases that are characterized by  $^3He/^4He$  ratios  $< 1.6$  Ra (Figure 3a). This group includes other gas emissions along the eastern coast (Bahía Concepción and El Chorro) and along the western coast and northern portion of the BCP (e.g., Punta Banda, Uruapan, San Carlos, Sierra Juárez, Agua Caliente, Valle de Guadalupe, San Valente, and San Antonio; Figure 1 and Table S2), which were not studied in this work. None of these gas emissions showed pure crustal  $^3He/^4He$  ratios (0.01–0.05 Ra; Morrison & Pine, 1955), indicating a clear contribution from the mantle or magma-derived  $^3He$  mixing

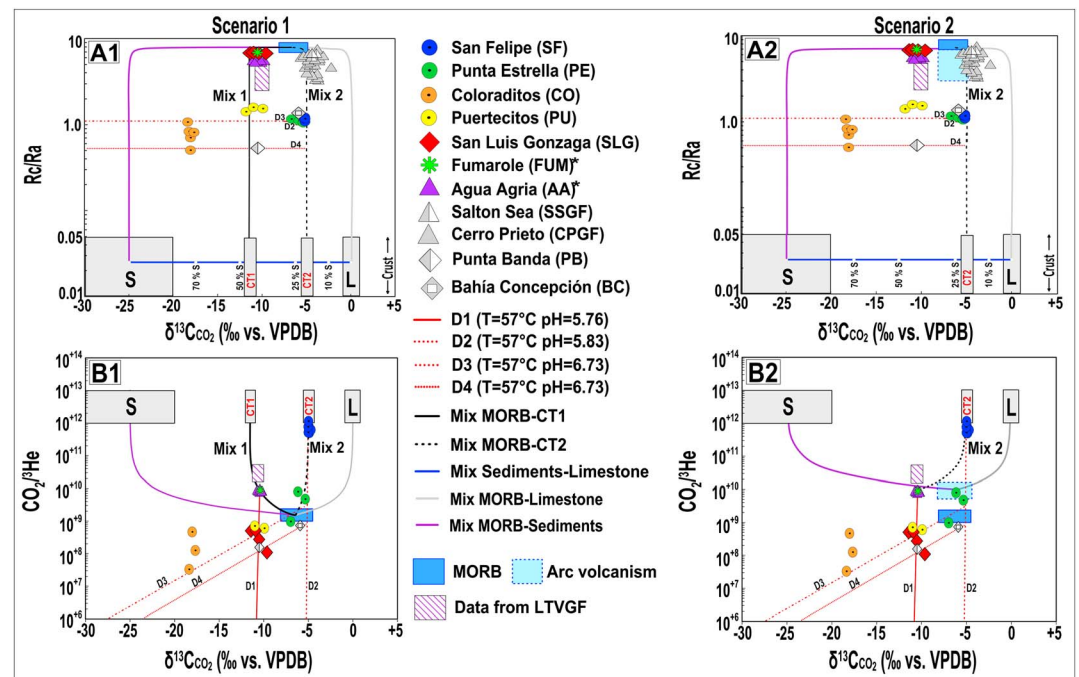


**Figure 6.** Combined plots  $Rc/Ra$  versus  $\delta^{13}C_{CO_2}$  (6a1 and 6a2) and  $CO_2/{}^3He$  versus  $\delta^{13}C_{CO_2}$  (6b1 and 6b2). Plots 6a1 and 6b1 refer to interpretative scenario 1, while 6a2 and 6b2 to scenario 2 (see text for details). The MORB range is the same as in previous figures. L (limestone) and S (sediments) were defined from Sano and Marty (1995) and are included within the crust field, as defined by Morrison and Pine (1955). The crustal terms CT1 and CT2 consist of ~46% and ~20% organic sediments added to a pure limestone rock. The distinction between colored and gray symbols is as in Figure 1 caption. The mixing (Mix 1 and Mix 2) and  $CO_2$  dissolution paths are the same as in Figure 4. See the text for further details. The field arc volcanism was taken from Hilton et al. (2002). The distinction between colored and gray symbols is as in Figure 1 caption. The reported literature data are as follows: SSGF from Mazzini et al. (2011); CPGF from Birkle et al. (2016), Pinti et al. (2018) and Richard et al. (2019); and LTVGF from Birkle et al. (2016) and Richard et al. (2019). VPDB = Vienna Pee Dee Belemnite.

with crustal fluids (see section 5.3). Geographically, these gases are located in continental areas where volcanism is absent or has ceased long time ago. Along the eastern coast of the BCP, the highest  ${}^3He/{}^4He$  values were measured in Puertecitos gases (1.6 Ra), which could be linked to two possible scenarios: (a) the presence of a deep-seated, cooling magma chamber that is still degassing and is related to Late Pliocene felsic volcanism between 3.2 and 2.5 Ma (Martín-Barajas et al., 1995) or (b) the occurrence of more recent submarine volcanism in the GoC. The Ulloa99 high-resolution seismic lines, which are located east of Puertecitos, indicate that the continental shelf is cut by a high-density array of normal and oblique faults (Martín-Barajas et al., 2013; Persaud et al., 2003), and the edge of the shelf includes a prominent rhyolite volcano that is 13.5 km SW of Puertecitos.

The lowest  ${}^3He/{}^4He$  values within this group (i.e., Coloraditos with 0.5–1.1 Ra) are comparable to those of the gas emissions in the northern BCP (i.e., Agua Caliente, Uruapan, Valle de Guadalupe, San Antonio, San Carlos, Sierra Juárez, and San Valente) and to those of the El Chorro site, which is located at the southern end of the peninsula (Figure 1). These hydrothermal springs were interpreted as originating in active fault zones, where the strong release of radiogenic  ${}^4He$  occurs (Polyak et al., 1991; Vidal et al., 1981).

### 5.1.2. Origin of $CO_2$

To constrain the origin of  $CO_2$ , we integrate and compare the  $CO_2$  concentration and  $\delta^{13}C$  with  ${}^3He/{}^4He$  measurements to evaluate the contributions from mantle, organic, and limestone sources of  $CO_2$  (e.g., Sano & Marty, 1995; Figures 6a1, 6b1 and 6a2, 6b2).

The magmatic gases (Agua Agria, Fumarole, and San Luis Gonzaga) were  $CO_2$  dominated, except at San Luis Gonzaga, which showed variable chemistry with  $CO_2$  from ~17% to ~55% and  $CH_4$  from ~41% to ~77% (Figure 2b). The  $\delta^{13}C_{CO_2}$  of these magmatic gases varied between  $-9.6\text{‰}$  and  $-11.3\text{‰}$ , irrespective

of their chemistry (Figure 4). However, the  $\text{CO}_2/{}^3\text{He}$  ratios spanned a wide range from  $\sim 1 \cdot 10^8$  to  $\sim 1 \cdot 10^{10}$  (Figure 6b1), only partially overlapping the typical MORB signature ( $\text{CO}_2/{}^3\text{He} = 2 \cdot 10^9$ ; Sano & Marty, 1995).

As argued before, the  ${}^3\text{He}/{}^4\text{He}$  values that were measured in magmatic gases were slightly below the MORB range (Figure 6a1), suggesting a strong mantle contribution (see section 5.3). However, the observed  $\delta^{13}\text{C}_{\text{CO}_2}$  values were either lower than (i.e., lighter than) the typical MORB range ( $-8\text{‰} < \delta^{13}\text{C}_{\text{CO}_2} < -4\text{‰}$ ; Des Marais & Moore, 1984; Marty et al., 1989; Sano & Williams, 1996) and below the few data ( $-6\text{‰} < \delta^{13}\text{C}_{\text{CO}_2} < +2\text{‰}$ ) that were available from the hydrothermal fluids at the rift centers in the GoC (e.g., the Guaymas basin; Galimov & Simoneit, 1982; Welhan & Lupton, 1987). This observation implies two possible scenarios:

1. magmatic gases from the BCP do not reflect a pure mantle signature but underwent crustal contamination at a local scale, which significantly modified the pristine carbon isotope composition toward more negative  $\delta^{13}\text{C}_{\text{CO}_2}$  values (Figures 4a1, 4b1 and 6a1, 6b1); or
2. magmatic gases are representative of the local mantle that is contaminated by sediments containing a small fraction of organic C that subducted with the Farallon plate up to  $\sim 12$  Ma ago (Atwater, 1970; Stock & Lee, 1994; Figures 4a2, 4b2 and 6a2, 6b2).

When plotting  $\delta^{13}\text{C}_{\text{CO}_2}$  versus  $\text{CO}_2/{}^3\text{He}$ , the first scenario could only be reproduced by assuming binary mixing between the mantle and a hypothetical crustal term (hereafter CT1), with  $\delta^{13}\text{C}_{\text{CO}_2} = -11.5\text{‰}$ ,  $\text{He}/\text{CO}_2 \sim 1 \cdot 10^{-7}$ ,  $\text{CH}_4/\text{CO}_2 \sim 1$ , and  $\text{CO}_2/{}^3\text{He} \sim 1 \cdot 10^{13}$  (Mix 1, Figures 4b1 and 6b1). The CT1 end-member would correspond to a  $\sim 46\%$  addition of organic sediments to a typical marine limestone (Figure 6b1). This hypothesis is consistent with  $\delta^{13}\text{C}_{\text{CO}_2}$  values below the MORB range ( $-16.4\text{‰} < \text{CO}_2 < -10.9\text{‰}$ ) at variable  $\text{CO}_2/\text{CH}_4$  values in sediment gases from a drilled site (477 DSDP Hole) in the rift of the GoC, specifically, near the Guaymas basin (Figure 4b1, Galimov & Simoneit, 1982; Welhan & Lupton, 1987). These gases are thought to be produced by high-temperature hydrocarbon oxidation and/or the thermogenic alteration of organic matter during magmatic sill intrusions into a thick horizon of organic-rich sediments. Lizarralde et al. (2010) recognized a large area that extends 50 km to the NW and 40 km to the SW of the axis of the spreading center in the northern Guaymas basin, which is characterized by several discrete magmatic sill intrusions into these organic-rich sediments. Therefore, a small addition ( $\sim 0.1\%$ ) of the assumed crustal component (CT1) into a MORB-like source would reproduce the  $\text{CO}_2$  signature of the magmatic gases from the BCP (Mix 1, Figures 6a1 and 6b1).

Alternatively, the second scenario would involve the mantle beneath BCP having subduction-related features ( $\text{CO}_2/{}^3\text{He} \sim 1 \cdot 10^{10}$ , Hilton et al., 2002; Sano & Fischer, 2013;  $-8\text{‰} < \delta^{13}\text{C}_{\text{CO}_2} < -4\text{‰}$ , Des Marais & Moore, 1984; Marty et al., 1989; Sano & Williams, 1996) and having been contaminated by the recycling of sediments containing a small ( $< 0.1\%$ ) fraction of organic C (Figures 6a2 and 6b2) that lowered the  $\delta^{13}\text{C}_{\text{CO}_2}$  toward the values measured in magmatic gases ( $\delta^{13}\text{C}_{\text{CO}_2} \sim -10.5\text{‰}$ ). In support of this hypothesis, we highlight the following.

1. Richard et al. (2019) found comparable  $\text{CO}_2/{}^3\text{He}$  and  $\delta^{13}\text{C}_{\text{CO}_2}$  values in Las Tres Virgenes geothermal field, and they interpreted these negative ratios as a result of organic matter-rich oceanic sediment contamination during Farallon plate paleo-subduction. The authors excluded the hypothesis of modern crustal contamination with organic matter, considering that the geothermal field is an extremely arid area and thus recharge water is likely depleted in organic matter (Birkle et al., 2016).
2. Magmatic gases in BCP show  ${}^3\text{He}/{}^4\text{He}$  values that never exceed  $7.3 \pm 0.6$  Ra (Figure 6a2), which is within the range suggested for typical arc volcanism (Hilton et al., 2002) and is actually lower than typical MORB values measured in the rift in the GoC ( ${}^3\text{He}/{}^4\text{He}$  up to 8.4 Ra, Castillo et al., 2002).
3. Previously published data on gas emissions located in the central and western part of BCP show similar negative  $\delta^{13}\text{C}_{\text{CO}_2}$  values (e.g., Punta Banda,  $-10.5\text{‰}$ ; Vidal et al., 1981), suggesting that this signature is present at regional scale implying a deep origin of  $\text{CO}_2$  rather than local contaminations.

In fact, the only magmatic gas emissions in BCP showing  $\delta^{13}\text{C}_{\text{CO}_2}$  values within typical MORB range are Salton Sea and Cerro Prieto geothermal fields, which are located in the northeastern part of the peninsula along the on land extension of the fracturing related to the rift in the GoC. Therefore, below this area, it is reasonable to suppose a flux of  $\text{CO}_2$  originated from the rift that has MORB-like features.

### 5.1.2.1. Secondary Processes That Modify the Chemistry and CO<sub>2</sub> Isotope Composition of Sampled Gases

Among the magmatic gases, the observed chemical variability of San Luis Gonzaga can be modeled through the partial dissolution of CO<sub>2</sub> in water, assuming a condensation process under equilibrium conditions as expressed by the Rayleigh (1896) equation:

$$\frac{Rv}{Rv_0} = f^{\alpha-1}$$

where  $Rv_0$  is the initial ratio of the bulk composition (e.g., He/CO<sub>2</sub>),  $Rv$  is the same instantaneous ratio in the residual gas phase ( $v$ ),  $f$  is the fraction of the residual gas phase, and  $\alpha$  is the fractionation factor determined by the solubility ratio of the species under consideration (e.g.,  $k_{\text{He}}/k_{\text{CO}_2}$ ). Henry's constant  $k_{\text{H}}$  for the considered gas species was calculated based on the thermodynamic approach proposed by Fernandez-Prini et al. (2003) and references therein, and considering the temperature conditions that we assumed and reported below.

Similar to gas chemistry, the isotopic composition of gaseous CO<sub>2</sub> ( $\delta^{13}\text{C}_{\text{CO}_2}$ ) changes as a result of its dissolution in water and the isotopic fractionation between gaseous and dissolved inorganic CO<sub>2</sub> [CO<sub>2</sub> (aq)] (e.g., Vogel, 1970). CO<sub>2</sub> (aq) is referred as dissolved inorganic C (DIC) and is equal to the sum of the aqueous species H<sub>2</sub>CO<sub>3</sub>, HCO<sub>3</sub><sup>-</sup>, and CO<sub>3</sub><sup>2-</sup>. The molar fraction of each C species depends on the water temperature and pH. The fractionation process can be modeled using the Rayleigh equation as follows (Clark & Fritz, 1997):

$$\delta^{13}\text{C}_{\text{CO}_2} = (\delta^{13}\text{C}_{\text{CO}_2})_0 + \epsilon \ln(f)$$

where  $(\delta^{13}\text{C}_{\text{CO}_2})_0$  is the initial CO<sub>2</sub>-isotope composition,  $f$  is the fraction of the residual gas phase, and  $\epsilon$  is the fractionation factor between DIC and gaseous CO<sub>2</sub> (CO<sub>2(g)</sub>). This fractionation factor is obtained by summing up the fractionation factors of dissolved C species and CO<sub>2(g)</sub> taking into account their molar fraction with respect to DIC (Zhang et al., 1995).

For San Luis Gonzaga we assumed dissolution of CO<sub>2</sub> in a water at  $T = 57^\circ\text{C}$  and  $\text{pH} = 5.76$  (D1, Figures 4 and 6). The fractionated gases from San Luis Gonzaga are compatible with those from Fumarole and Agua Agria, confirming that the variability in the chemistry at San Luis Gonzaga does not reflect any mixing but it is likely the result of dissolution of CO<sub>2</sub> in water. Under these conditions,  $\delta^{13}\text{C}$  does not fractionate, while elemental ratios such as He/CO<sub>2</sub>, CH<sub>4</sub>/CO<sub>2</sub>, and CO<sub>2</sub>/<sup>3</sup>He can be strongly modified.

The hydrothermal gases revealed different compositions to the magmatic gases in terms of both the chemistry and the carbon isotope composition (Figure 4). Only San Felipe and Punta Estrella gases were CO<sub>2</sub> dominated, while Puertecitos and Coloraditos were N<sub>2</sub> and CH<sub>4</sub> dominated, respectively (Figure 2b). The  $\delta^{13}\text{C}_{\text{CO}_2}$  values varied between  $\sim -18\text{‰}$  and  $\sim -5\text{‰}$  (Figures 4 and 6). The CO<sub>2</sub>/<sup>3</sup>He ratio varied from  $\sim 3 \cdot 10^7$  to  $\sim 1 \cdot 10^{12}$  (Table S1 and Figures 6b1 and 6b2). Considering the variability of the hydrothermal gases in terms of chemistry and  $\delta^{13}\text{C}_{\text{CO}_2}$ , only gases from San Felipe (CO<sub>2</sub> > 98.5%) can be considered as a starting point to constrain the origin of CO<sub>2</sub>. These gases had  $\delta^{13}\text{C}_{\text{CO}_2} \sim -5\text{‰}$  and CO<sub>2</sub>/<sup>3</sup>He  $\sim 5 \cdot 10^{11}$ . Although the  $\delta^{13}\text{C}_{\text{CO}_2}$  values of San Felipe were within the typical MORB range ( $-8\text{‰} < \delta^{13}\text{C}_{\text{CO}_2} < -4\text{‰}$ ; Des Marais & Moore, 1984; Marty et al., 1989; Sano & Williams, 1996), the CO<sub>2</sub>/<sup>3</sup>He values ( $4.9 \cdot 10^{11}$ – $1.19 \cdot 10^{12}$ ) were 2 orders of magnitude higher than those in the mantle, strongly indicating the addition of crustal carbon (Figures 6b1 and 6b2). This evidence matches findings from the <sup>3</sup>He/<sup>4</sup>He ratios (1.08–1.16 Ra), which indicate that these gases reflect mixing between a magmatic/mantle and a crustal term (Figures 3a and 6a1). Although no clues can clearly constrain this hypothesis, we infer that the excess CO<sub>2</sub> originated from binary mixing between a MORB-like source ( $-8\text{‰} < \delta^{13}\text{C}_{\text{CO}_2} < -4\text{‰}$ ; Des Marais & Moore, 1984; Marty et al., 1989; Sano & Williams, 1996 and CO<sub>2</sub>/<sup>3</sup>He =  $2 \cdot 10^9$ ; Sano & Marty, 1995) and another crustal term (hereafter CT2) with  $\delta^{13}\text{C}_{\text{CO}_2} = -4.9\text{‰}$ , He/CO<sub>2</sub>  $\sim 1 \cdot 10^{-7}$ , CH<sub>4</sub>/CO<sub>2</sub>  $\sim 5 \cdot 10^{-5}$ , and CO<sub>2</sub>/<sup>3</sup>He  $\sim 1 \cdot 10^{13}$  (Mix 2, Figures 4a1, 4b1 and 6a1, 6b1). CT2 could have originated from crustal CO<sub>2</sub>-dominated reservoirs with a  $\sim 20\%$  addition of organic sediments to pure limestone (Figures 6a1 and 6b1).

In the hypothesis of a mantle beneath BCP contaminated by the Farallon plate paleo-subduction, as above discussed, the excess of CO<sub>2</sub> measured in gases from San Felipe would be explained similarly. The only

exception would be in the mantle source features that would have  $\delta^{13}\text{C}_{\text{CO}_2} = -10.5\text{‰}$  and  $\text{CO}_2/{}^3\text{He} = 1 \cdot 10^{10}$  instead of typical MORB values (Figures 6a2 and 6b2).

The other hydrothermal gases (e.g., Punta Estrella, Bahía Concepción, Coloraditos, Punta Banda, and Puertecitos) can be explained as the result of one or more overlapping (multistep) processes that involved the partial dissolution of  $\text{CO}_2$  in water, by assuming the condensation process above (Figures 4 and 6). In fact, the gases from Punta Estrella and Bahía Concepción can be modeled by the dissolution of San Felipe-type gases in water at  $T = 57\text{ °C}$  and  $\text{pH} = 5.83$  (e.g., D2, Figures 4 and 6). Under these conditions, the maximum range of  $\delta^{13}\text{C}$  fractionation is  $0.4\text{‰}$  (at a residual fraction  $f = 0$ ), while elemental ratios such as  $\text{He}/\text{CO}_2$ ,  $\text{CH}_4/\text{CO}_2$ , and  $\text{CO}_2/{}^3\text{He}$  are strongly modified. The gases from Puertecitos, Coloraditos, and Punta Banda could have resulted from the further partial dissolution of  $\text{CO}_2$  in water at  $T = 57\text{ °C}$  and  $\text{pH} = 6.73$ , starting from a similar composition to that of the Punta Estrella gases or slightly more fractionated gases (e.g., D3 and D4, Figures 4 and 6). Under these conditions,  $\delta^{13}\text{C}$  strongly fractionates compared to elemental ratios such as  $\text{He}/\text{CO}_2$ ,  $\text{CH}_4/\text{CO}_2$ , and  $\text{CO}_2/{}^3\text{He}$ .

Even if we do not know the saturation state of these thermal waters with respect to carbonate minerals (e.g., calcite and dolomite), we cannot rule out the possibility that under these conditions part of  $\text{CO}_2$  loss and  $\delta^{13}\text{C}$  fractionation is due to the precipitation of calcite/dolomite together with  $\text{CO}_2$  dissolution. This hypothesis would be supported by the findings of Gilfillan et al. (2009) and Ray et al. (2009), who observed the loss of  $\text{CO}_2$  (up to 18%) due to the precipitation of carbonated minerals and the subsequent decrease in the  $\text{CO}_2/{}^3\text{He}$  ratio. We point out that gases from Punta Banda could also result from dissolution of  $\text{CO}_2$  in a water at  $T = 57\text{ °C}$  and  $\text{pH} = 5.76$  (D1, Figures 4 and 6), as assumed for San Luis Gonzaga magmatic gases. The multi-step partial dissolution of  $\text{CO}_2$  plus calcite precipitation in water seems to be a reasonable assumption because gases that rise within the crust often encounter one or more aquifers with different physical-chemical conditions before escaping at the surface (e.g., Caracausi et al., 2003; Dubacq et al., 2012; Gilfillan et al., 2009; Ray et al., 2009).

### 5.1.3. Origin of Methane

Methane in magmatic and hydrothermal gases may have a *biotic* origin, which is linked to either the thermal degradation (thermogenic methane) or microbial transformation (biogenic methane) of organic matter. Alternatively, *abiotic* methane may be produced by chemical reactions that involve gaseous species (mainly  $\text{H}_2$  and  $\text{CO}$ ) over a wide range of temperatures and in the absence of organic compounds. Other possible inorganic processes that can produce abiotic methane were listed and described in more detail in Etiope and Sherwood-Lollar (2013). The stable isotopes (both C and H) of methane and the relative abundance of methane ( $\text{C}_1$ ) and the other heavier hydrocarbons ( $\text{C}_2$ , Ethane and  $\text{C}_3$  Propane) have been successfully used to distinguish between thermogenic and biogenic methane.

Thermogenic methane is generally characterized by  $\delta\text{D}_{\text{CH}_4}$  values below  $-150\text{‰}$ ,  $\delta^{13}\text{C}_{\text{CH}_4}$  values of  $-50\text{‰}$  to  $-30\text{‰}$ , and  $\text{C}_1/(\text{C}_2 + \text{C}_3)$  ratios below 100 (Figures 5a and 5b). Biogenic-produced methane (either via acetate fermentation or  $\text{CO}_2$  reduction) is enriched in light carbon isotopes (usually  $\delta^{13}\text{C}_{\text{CH}_4} < -50\text{‰}$ ) and lighter alkanes, producing  $\text{C}_1/(\text{C}_2 + \text{C}_3)$  ratios from  $10^3$  to  $10^5$  (Figure 5a). On the other hand, *abiotic* methane, which is associated very often but not exclusively with high-temperature hydrothermal/volcanic emissions, generally shows enrichment in heavy isotopes, with  $\delta^{13}\text{C}_{\text{CH}_4}$  around  $-23 \pm 6\text{‰}$ ,  $\delta\text{D}_{\text{CH}_4}$  values between  $-50\text{‰}$  and  $-150\text{‰}$  and  $\text{C}_1/(\text{C}_2 + \text{C}_3)$  ratios from  $1 \cdot 10^2$  to  $3 \cdot 10^3$ .

Therefore, two classification diagrams are commonly used to identify the origin of methane in natural gases:

1. the *Bernard diagram* (Bernard et al., 1978, Figure 5a), which correlates  $\delta^{13}\text{C}_{\text{CH}_4}$  and the  $\text{C}_1/(\text{C}_2 + \text{C}_3)$  ratio (*Bernard parameter*), where  $\text{C}_1$  stands for  $\text{CH}_4$ ,  $\text{C}_2$  for  $\text{C}_2\text{H}_6$ , and  $\text{C}_3$  for  $\text{C}_3\text{H}_8$ ;
2. the  $\delta\text{D}_{\text{CH}_4}$  versus  $\delta^{13}\text{C}_{\text{CH}_4}$  diagram, which was proposed by Schoell (1980) and updated by Etiope and Schoell (2014) (Figure 5b).

These interpretative plots have been successfully used by many authors to distinguish thermogenic methane from biogenic methane (either acetate fermentation or  $\text{CO}_2$  reduction). Sometimes they were of limited utility since secondary postgenetic processes (e.g., oxidation, mixing, migration, and selective hydrocarbon sorption onto particles) may alter the pristine molecular and/or isotope composition, thus overprinting the hydrocarbon formation process. Moreover, to the present knowledge, the fields relative to abiotic methane have been not well constrained thus making difficult the identification of abiotic methane.

In the Bernard diagram (Figure 5a), the collected samples were plotted together with the other samples from BCP peninsula and the gas from the seafloor hydrothermal system of the Guaymas basin. As a reference, in the same plot, we have also reported the fields relative to volcanic gas (McCollom & Seewald, 2007) and the gas from the EPR (Welhan & Craig, 1983). The collected samples fall far from the expected molecular and isotopic composition for the four identified end-members (i.e., biogenic, thermogenic, volcanic, and EPR type). Punta Estrella had an intermediate composition showing a typical Bernard parameter for biogenic methane with heavier  $\delta^{13}\text{C}$  values or a typical Bernard parameter for thermogenic methane with lighter  $\delta^{13}\text{C}$  values. San Luis Gonzaga showed intermediate compositional values between thermogenic methane and methane that is associated with volcanic gases/EPR-type methane. Coloraditos and Puertecitos were characterized by positive  $\delta^{13}\text{C}$  values and  $C_1/(C_2 + C_3)$  ratios below 205.

In Figure 5b, Punta Estrella, Agua Agria, and San Luis Gonzaga showed a typical isotope signature for thermogenic methane, with Agua Agria and San Luis Gonzaga exhibiting a slight  $\delta^{13}\text{C}$  shift toward more positive values. Finally, Coloraditos and Puertecitos were characterized by positive  $\delta\text{D}$  values ( $>100\text{‰}$ ).

Based on the molecular abundances and isotope signatures, we propose that the methane in Punta Estrella, Agua Agria, and San Luis Gonzaga is thermogenic in origin and likely formed via the thermal cracking of organic matter in sediments and a magmatic heat source. The Bernard parameter at Punta Estrella, higher than those of typical thermogenic methane, suggests to be the result of molecular fractionation at a shallower level during gas migration (Etiope et al., 2009) from the reservoir toward the surface. Coloraditos and Puertecitos seemed to be affected by severe secondary oxidation (microbial/inorganic) processes. If we consider the anaerobic oxidation of methane as a simple closed-system Rayleigh distillation (Whiticar, 1999), with  $\epsilon_{\text{C-methane}} = 13$  and  $\epsilon_{\text{D-methane}} = 97$  as fractionation factors for carbon and hydrogen, respectively (Coleman et al., 1981), and assuming a similar initial  $\text{CH}_4$  isotope signature to Punta Estrella ( $\delta\text{D}_{\text{CH}_4} = -165\text{‰}$  and  $\delta^{13}\text{C}_{\text{CH}_4} = -41,8\text{‰}$ ), the 96% and 99.5% oxidation of  $\text{CH}_4$  would lead to a composition that is consistent with Coloraditos and San Felipe gas emissions, respectively (Figure 5b).

A thermogenic origin for the methane in the BCP has been already proposed by several authors (e.g., Mazzini et al., 2011; Welhan & Lupton, 1987) for the Salton Sea and Cerro Prieto geothermal fields and for some sediment gas that is released from the Guaymas basin. All these sites have a nonnegligible primordial mantle-derived  $^3\text{He}$  contribution ( $^3\text{He}/^4\text{He}$  ratios from 4.6 to 7 Ra) because of volcanism that is associated with the formation and development of the rift in the GoC. In the San Luis Gonzaga and Agua Agria samples, which have the largest magmatic component ( $>5.1$  Ra), the contribution from abiogenic methane, which could be derived from (i) a synthesis of methane from CO and/or  $\text{CO}_2$  at high temperature, or (ii) the respeciation of C-H-O fluids in late magmatic stages or (iii) Fischer-Tropsch-type synthesis reactions (Etiope & Sherwood-Lollar, 2013 and references therein), cannot be excluded. In fact, San Luis Gonzaga and Agua Agria show compatible chemical and isotope compositions with abiogenic EPR-type methane ( $\delta^{13}\text{C}_{\text{CH}_4}$  around  $-20\text{‰}$ ,  $\delta\text{D}_{\text{CH}_4}$  between  $-150$  and  $-50\text{‰}$ , and Bernard parameter between 100 and 1000; Figures 5a and 5b). To further support our approach, the San Luis Gonzaga gas composition is similar to that of fluids that are emitted in the Baogutu hydrothermal zone (Figure 5b), for which an abiogenic origin through Fischer-Tropsch reactions has been proposed (e.g., Cao et al., 2014).

## 5.2. Relationship Between $^3\text{He}/^4\text{He}$ and Crustal Thickness

The variability of  $^3\text{He}/^4\text{He}$  within the BCP gas manifestations indicates different extents of mantle/magmatic degassing. To examine the gases that are emitted within the peninsula in the context of local tectonic and geodynamic settings, we investigate the relationship between the  $^3\text{He}/^4\text{He}$  ratio and the crustal thickness according to seismic data from a local network along two main profiles where the emissions are located (Figures 7a and 7b). We expect that high crustal thickness enhances the production of  $^4\text{He}$  and lowers the  $^3\text{He}/^4\text{He}$  ratio in surface gas emissions. However, no exact correspondence exists between the gas emissions and seismic-network stations, so our consideration must be taken as general.

The first profile moves from WSW to ENE and is located in the northern BCP (Figures 7a and 7c). As expected, the lowest  $^3\text{He}/^4\text{He}$  values (0.1–0.6 Ra) in the central and westernmost areas (i.e., Punta Banda, San Carlos, Uruapan, San Valente, San Antonio, Valle de Guadalupe, and Agua Caliente) corresponded with the highest crustal thickness ( $>30$  km; Figure 7a), showing a good relationship. In fact,



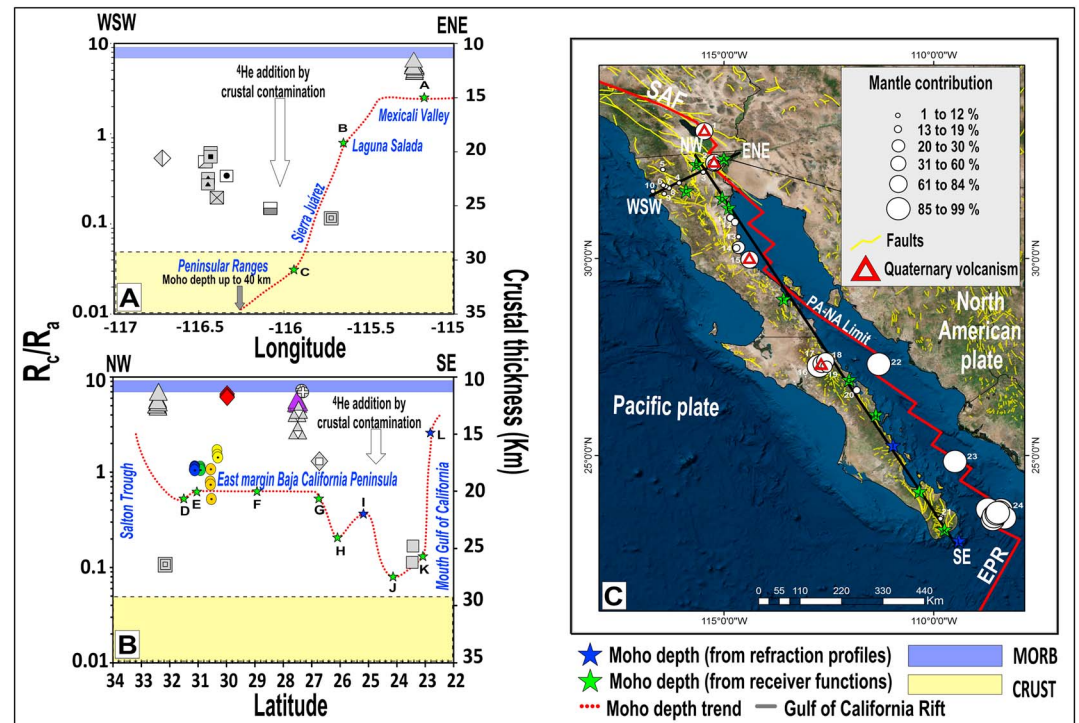


**Figure 7.** Combined figure that shows the relationship between  $R_c/R_a$  and the crustal thickness along two profiles (WSW-ENE [7a] and NW-SE [7b]) and the mantle contribution to gas emissions from the BCP and GoC (7c). The legend and data used are the same as in Figure 1 caption. (7a)  $R_c/R_a$  versus the longitude of gas emissions along the WSW-ENE profile (black solid line). The crustal thickness was taken from receiver-function profiles based on the following works: A and B represent Mexicali Valley and Laguna Salada's crustal thickness (Ramírez-Ramos et al., 2015), and C represents Agua Blanca station (Persaud et al., 2007). (7b)  $R_c/R_a$  versus the latitude of gas emissions along the NW-SE profile (black solid line). The crustal thickness was taken from receiver functions and refraction profiles based on the following: D, F, and J are the El Chintero, Bahía de los Ángeles, and La Paz stations, respectively (Fernández & Pérez-Campos, 2017); E is the San Felipe station (Reyes et al., 2001); G, H, and K are the Bahía Concepción, Loreto, and Los Cabos stations, respectively (Persaud et al., 2007); I and L are the refraction profile data (Lizarralde et al., 2007). In both graphs, the Moho trend (red dotted line) was interpolated because of gaps in data from some transect segments. The distinction between colored and gray symbols is as in Figure 1 caption. (7c) Map of the mantle contribution percentages to gas emissions in the BCP and GoC. The mantle contribution was calculated considering the  $^3\text{He}/^4\text{He}$  value of Alarcón lavas as the mantle end-member ( $\sim 8.4 \pm 0.14 R_a$ ; Castillo et al., 2002). The mantle and crust fields were established from Graham (2002) and Morrison and Pine (1955), respectively. The white numbers indicate the location of gas emissions as follows: 1, Salton Sea geothermal field; 2, Cerro Prieto geothermal field; 3, Sierra Juárez; 4, San Valente; 5, Valle de Guadalupe; 6, Agua Caliente; 7, San Carlos; 8, San Antonio; 9, Uruapan; 10, Punta Banda; 11, San Felipe; 12, Punta Estrella; 13, Coloraditos; 14, Puertecitos; 15, San Luis Gonzaga; 16, La Virgen lavas; 17, Agua Agria; 18, Fumarole; 19, Las Tres Vírgenes geothermal field; 20, Bahía Concepción; 21, El Chorro; 22, Guaymas basin; 23, Pescadero basin; and 24, Alarcón basin. The faults represented in the figure were taken from the cartographic bases of the Instituto Nacional de Estadística y Geografía (INEGI) (2013), available in <https://www.inegi.org.mx> and from U.S. Geological Survey (2006) available in <http://earthquakes.usgs.gov/regional/qfaults>. BCP = Baja California Peninsula; GoC = Gulf of California.

seismic studies (e.g., Ichinose et al., 1996; Lewis et al., 2001, 2000) indicated a crustal thickness up to 40 km along the Peninsular Ranges and the progressive thinning of the crust toward the eastern margin of the BCP and within the GoC (see also Figure 8). Accordingly, the highest  $^3\text{He}/^4\text{He}$  values (3.3–7.3  $R_a$ ) were measured in the easternmost portion of the profile (i.e., Cerro Prieto geothermal field) to Mexicali Valley, corresponding with the lowest crustal thickness ( $\sim 15$  km; Figure 7a) as reported by Ramírez-Ramos et al. (2015). These authors also reported a crustal thickness of 19 km beneath Laguna Salada (Point B in the WSW-ENE profile, Figure 7a).

The second profile moves from NW to SE and is located along the eastern coast of the BCP (Figures 7b and 7c). This profile, especially in the northern and central areas, lacks a clear relationship between the  $^3\text{He}/^4\text{He}$  ratio and crustal thickness (Figure 7b). In fact, the  $^3\text{He}/^4\text{He}$  ratio from San Felipe (Station E) to Bahía

Concepción (Station G) varied from 0.5 to 7.0 Ra at almost constant crustal thickness (~20 km, Figure 7b). A certain relationship began in the southern portion of the profile, where volcanic activity is missing and the crustal thickness increases to ~26 km (Persaud et al., 2007), with the  $^3\text{He}/^4\text{He}$  ratio lowering to 0.1–0.2 Ra at El Chorro (Polyak et al., 1991; Figure 7b).

### 5.3. Relationship Between $^3\text{He}/^4\text{He}$ and Active Faults

Although the knowledge of the local structural setting is not well defined, we investigated the mantle contribution in gases emitted from the BCP. The aim was to recognize the possible relationship between the location of gas emissions and active volcanism, and to infer the presence and the role of active faults able to drive mantle-derived fluids toward the surface. For this purpose, in Figure 7c we report the main known fault systems within the peninsula. The mantle contribution is calculated with the following relation:

$$Mc = \frac{\left[\frac{\text{Rc}}{\text{Ra}}\right]_s}{\left[\frac{\text{Rc}}{\text{Ra}}\right]_m} \cdot 100$$

where Mc is the mantle contribution,  $(\text{Rc}/\text{Ra})_s$  is the  $^3\text{He}/^4\text{He}$  measured in each gas sample, and  $(\text{Rc}/\text{Ra})_m$  is the hypothetical  $^3\text{He}/^4\text{He}$  ratio of the local mantle. For our calculation, we assumed that the mantle beneath the BCP has MORB-like features with  $^3\text{He}/^4\text{He} = 8.4 \pm 0.14$  Ra (first scenario in section 5.1.2), which is the highest measured value in fluid inclusions of Alarcon basin basalts (Castillo et al., 2002) in the rift of the GoC (Figure 7c). The results of this calculation are reported in Table S2. We highlight that the calculated percentages could be even higher of ~10% in the hypothesis of a local mantle with  $^3\text{He}/^4\text{He} = 7.3$  Ra because of the contamination by Farallon plate paleo-subduction (second scenario in section 5.1.2).

The highest percentages of mantle contribution are observed at Cerro Prieto geothermal field (~87%), San Luis Gonzaga (~82%), Salton Sea geothermal field (~79%), and Las Tres Virgenes geothermal field (~68%), which are located in zones of recent volcanic activity (Figure 7c, García-Sánchez et al., 2017; Robinson et al., 1976; Schmitt et al., 2012, 2013; Wright et al., 2015).

Despite the lack of active volcanism in the region, the hydrothermal gases along the NW-SE profile are characterized by a significant mantle contribution (up to ~21%) that suggests the presence of active faults and the proximity of the active rift of the GoC (Figure 1).

Finally, the lowest mantle contribution (~1–7%) was observed in the central and westernmost portions of the WSW-ENE profile (i.e., Punta Banda, Uruapan, San Carlos, San Valente, Valle de Guadalupe, San Antonio, Agua Caliente, and Sierra Juárez) and the southernmost portion of the NW-SE profile (i.e., El Chorro). These zones are characterized by the absence of magmatism, and the small percentage of mantle fluids presumably rise because of the presence of local, shallow faults (e.g., Tres Hermanas, Agua Blanca, and San Miguel) in a zone of high crustal thickness (>25 km, Figures 7a and 7c).

Instead, the easternmost portion of the WSW-ENE profile (close to Cerro Prieto geothermal field) and most of the NW-SE profile (i.e., San Felipe, Punta Estrella, Coloraditos, Puertecitos, San Luis Gonzaga, Agua Agria, Fumarole, and Bahía Concepción) is characterized by a higher mantle contribution (>7%).

It is noteworthy that a typical crustal  $^3\text{He}/^4\text{He}$  ratio (0.01–0.05 Ra; Morrison & Pine, 1955) has not been measured in any gas emission from the BCP, indicating that likely the BCP is characterized by active fault systems and/or magmatism that favors the ascension of mantle-derived fluids that mixed with fluids from the crust.

Therefore, a better definition of the structural setting of the BCP is a research priority, not only where magmatism is absent but also in the active volcanic systems (Tardani et al., 2016). Detailed structural observations should be addressed first to try to map these tectonic lineaments enhancing the rising of the mantle fluids, and second to understand the role played by these high vertical permeability zones in promoting or limiting secondary crustal processes (mixing, dissolution, and residence times), which affect the final chemical and isotope composition of the fluids.

### 5.4. Conceptual Model

We highlighted the complexity of the processes (e.g., mixing with atmospheric gas, crustal contamination, and single or multistep gas-water interactions) that have occurred and, thus, modified the pristine

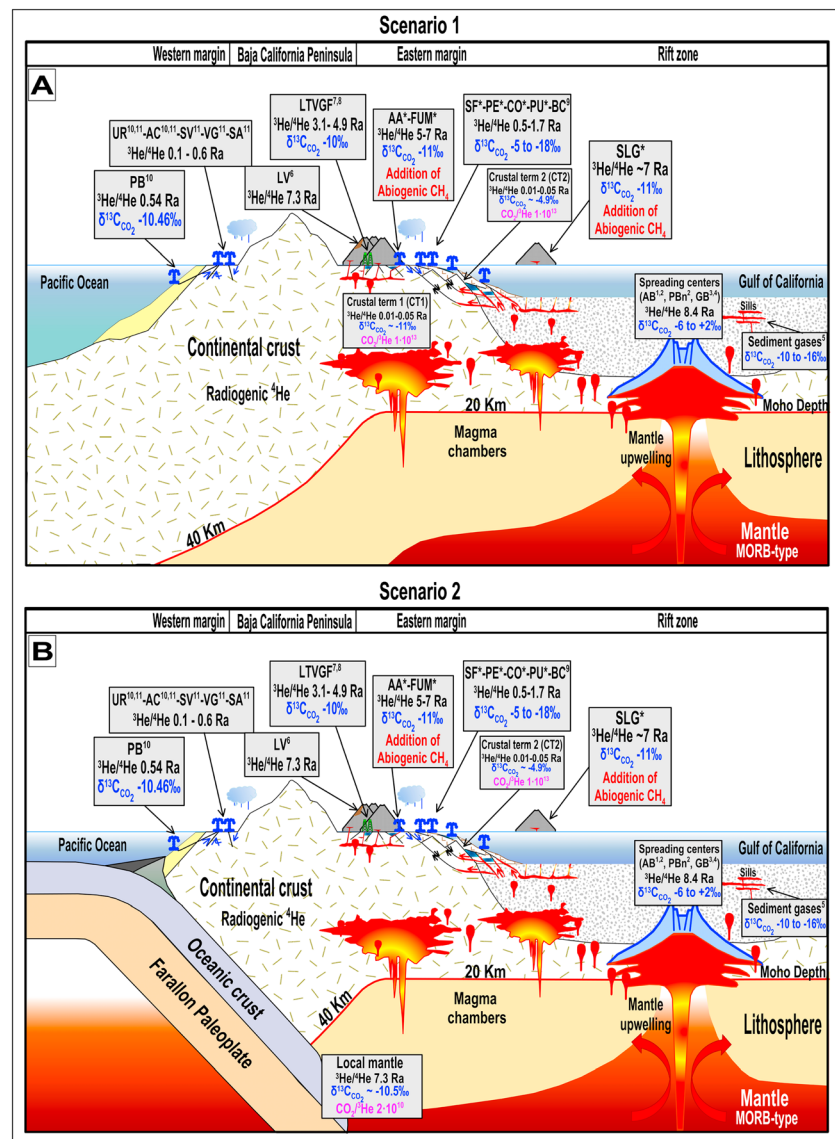


**Figure 8.** Conceptual models (not to scale) of mantle degassing in the BCP and GoC, based in two possible scenarios. (8a) Scenario 1 represents the process of crustal contamination with two crustal terms (CT1) and (CT2) that affect de hydrothermal and magmatic gases composition (see the text for further details). In this scenario it is assumed that the mantle beneath the BCP is similar to MORB. (8b) Scenario 2 represents a local mantle contaminated by the paleo-subduction of the Farallon plate and the sedimentary process associated. The angle of the subducted plate is not to scale. The subduction of Farallon plate beneath the BCP ceased at 12 Ma ago (Lonsdale, 1989; Stock & Hodges, 1989), and the volcanism in the eastern area of the BCP is not linked with this process but with rifting. In both figures the locations of the emissions in the eastern side do not follow a geographical pattern; this arrangement is only schematic. The crustal thickness beneath the BCP and GoC is based on findings by Ichinose et al. (1996), Lewis et al. (2000), and Lewis et al. (2001). The superscripts for the labels inside the boxes represent data from the following authors: 1, Castillo et al. (2002); 2, Spelz et al. (2015); 3, Lupton (1979); 4, Welhan and Lupton (1987); 5, Galimov and Simoneit (1982); 6, Schmitt et al. (2010); 7, Birkle et al. (2016); 8, Richard et al. (2019); 9, Forrest et al. (2005); 10, Vidal et al. (1981); 11, Polyak et al. (1991). An asterisk indicates data from this study. The blue and red arrows indicate meteoric recharge and circulation of fluids, respectively. The black arrows indicate the displacement of the faults (black lines), mainly normal and listrics.

signature of mantle/magmatic gases, resulting in the various compositions measured in the surface gases. Based on data from this study and a careful review of data from previous works, we reconstruct two conceptual models (Figure 8) that we regard as equally plausible. These models rationalize (1) the mantle features beneath the BCP and GoC, (2) the processes that modified the mantle signature and explain the different compositions of gases that are emitted at the surface, and (3) the timing of these processes.

Scenario 1 (Figure 8a): mantle beneath BCP has MORB-like features

1. The mantle beneath the GoC has typical MORB-like features, as suggested by the  $^3\text{He}/^4\text{He}$  value of 8.4 Ra in fluid inclusions from Alarcón basin basalts (Castillo et al., 2002) and the  $\delta^{13}\text{C}_{\text{CO}_2}$  values of  $\sim -6\%$  in hydrothermal fluids from Guaymas basin (Welhan & Lupton, 1987). These mantle features can be extended to the mantle beneath the BCP. However, more studies on fluid inclusions from volcanic rocks in the BCP and submarine gases along the GoC are necessary to better constrain the origin of mantle fluids.
2. Gases that rise from the mantle beneath the BCP through lithospheric faults or magmatic plumbing systems mix and contaminate within the crust with two distinct crustal terms (CT1 and CT2). The first (CT1) produces magmatic gases with  $\delta^{13}\text{C}_{\text{CO}_2}$  values that are more negative than typical MORB and  $^3\text{He}/^4\text{He}$  ratios that are slightly lower than the MORB range. This crustal term is inferred based on similar data that were measured in sediment gases from the Guaymas basin within the rift of the GoC (Galimov & Simoneit, 1982; Welhan & Lupton, 1987). The second (CT2) produces hydrothermal gases with  $\delta^{13}\text{C}_{\text{CO}_2}$  values that are comparable to those of MORB and  $^3\text{He}/^4\text{He}$  values that are well below the MORB range. For both crustal sources, we have no constraints on the depth at which the contamination occurs.

Scenario 2 (Figure 8b): Mantle beneath BCP is contaminated by paleo-subduction of the Farallon plate

1. The mantle beneath the GoC was contaminated by the recycling of sediments above the Farallon plate containing a very limited fraction of organic C that lowered  $^3\text{He}/^4\text{He}$  down to 7.3 Ra (values typical for arc volcanism, Hilton et al., 2002), shifted the  $\delta^{13}\text{C}_{\text{CO}_2} \sim -10.5\%$  (e.g., the values measured in Agua Agria, San Luis Gonzaga, and Fumarole) and increased the  $\text{CO}_2/{}^3\text{He}$  toward values ( $>2 \cdot 10^{10}$ ) higher than that typical of MORB-type gas.
2. Mantle gases rising through deep-rooted discontinuities or magmatic plumbing systems mix with crustal fluids ( $^4\text{He}$ -rich and  $^{13}\text{C}_{\text{CO}_2}$ -rich fluids) thus leading to almost pure  $\text{CO}_2$  hydrothermal gases (e.g., San Felipe) with  $\delta^{13}\text{C}_{\text{CO}_2}$  values close to  $-5\%$  and  $^3\text{He}/^4\text{He}$  values that are well below the MORB range ( $^3\text{He}/^4\text{He} < 1.6$  Ra).

Independent from Model 1 or Model 2, following the above mentioned crustal contamination processes, the chemistry and  $\delta^{13}\text{C}_{\text{CO}_2}$  values of both magmatic and hydrothermal gases at very shallow levels (presumably within 1–2 km) change through the partial dissolution of  $\text{CO}_2$  in water. Finally, the gases are slightly contaminated by the atmosphere at the subsurface or during sampling.

The origin of  $\text{CH}_4$  in gases from the BCP is thermogenic and likely related to the thermal cracking of organic matter in sediments, although abiotic methane (Etiope & Sherwood-Lollar, 2013 and references therein) in the magmatic gases cannot be excluded. The main heat source can be recognized along the rift fracture in both ocean basins and on-land areas (see Espinoza-Ojeda et al., 2017). Shallow postgenetic processes (molecular fractionation and the anaerobic oxidation of methane) likely affect the molecular and isotope composition of some hydrothermal gases.

Notably, both the conceptual models can explain the complexity of the chemical and the He-C systematic of most of the gases that are emitted within the BCP. The approach used in this work is general and can be applied to other continental areas where either magmatic or nonmagmatic gases are emitted. Indeed, Hrubcová et al. (2017) have used a similar approach for the case of the Western Eger Rift (central Europe).

## 6. Conclusions

This work constitutes a new and integrative compilation of  $^3\text{He}/^4\text{He}$ ,  $\delta^{13}\text{C}_{\text{CO}_2}$ ,  $\delta^{13}\text{C}_{\text{CH}_4}$ , and  $\delta\text{D}_{\text{CH}_4}$  isotopes in gas emissions from the BCP. This paper presents data for submarine, intertidal, and subaerial gas emissions along the eastern coast of the BCP and a careful review of existing information from other locations, including data for fluid inclusions and gases from spreading centers along the rift of the GoC. We summarize our main findings as follows:

1. Based on their  $^3\text{He}/^4\text{He}$  ratios, the gas emissions within the BCP have been classified as hydrothermal and magmatic gases.

2. Hydrothermal and magmatic gases show wide chemical and He-C isotope variability because of a complexity of processes within the crust magmatic and hydrothermal gases. These processes, occurring at different levels within the crust and with different timings, include mixing with local crustal fluids, dissolution of CO<sub>2</sub> in water, and atmospheric contamination.
3. The origin of methane is mainly thermogenic. Abiogenic methane production cannot be excluded, at least for magmatic gases. Some hydrothermal gases (San Felipe, Punta Estrella, Coloraditos, and Puertecitos) might undergo secondary postgenetic processes such as migration and oxidation, leading to unusual positive C and H isotope composition.
4. A comparative analysis between the <sup>3</sup>He/<sup>4</sup>He ratio and crustal thickness along two main profiles revealed that a good correlation only exists in the northern BCP (WSW-ENE direction), where lower <sup>3</sup>He/<sup>4</sup>He ratios (more radiogenic) are found in accordance with higher crustal thickness. Good <sup>3</sup>He/<sup>4</sup>He-crustal thickness agreement exists along this profile, including the Mexicali Valley area. On the contrary, this correlation is not as evident along the NW-SE profile (eastern coast), where the crustal thickness is quite homogenous (~20 km) but the <sup>3</sup>He/<sup>4</sup>He ratio shows great variability (0.5–7 Ra).
5. Based on <sup>3</sup>He/<sup>4</sup>He, all the gases that are emitted from the BCP have a mantle contribution that varies from at least ~1% to ~82%, depending on their location and the assumed <sup>3</sup>He/<sup>4</sup>He in the mantle. As expected, the highest mantle contribution (>60%) is found in magmatic gases emitted in zones of recent magmatic activity. Hydrothermal gases have a significantly lower mantle contribution than magmatic gases, although the former never show a pure crustal signature (0.01–0.05 Ra). This finding indicates that the BCP is likely intersected by active faults that are deeply rooted in the crust, favoring the ascension of mantle-derived fluids that have mixed with fluids in the crust.
6. We propose two possible models to infer the local mantle composition beneath the BCP: a typical MORB-like type, reflecting a composition similar to that of the gas released from the spreading centers of the GoC, or a MORB type contaminated by the recycling of sediments during the paleo-subduction of Farallon plate ended around 12 Ma ago. In addition, the models summarize the chemical and isotope variability in magmatic and hydrothermal gases that are emitted within the BCP and GoC, although these regions are distant.

#### Acknowledgments

This work was funded by the project 644-294 “Campana Intensiva de Exploración Geotérmica de las Cuencas Wagner, Consag, Delfin, Guaymas and Alarcón del Sistema de Rifts del Golfo de California” (CeMIEGeo) P03, CONACYT doctoral scholarship 308695 and project PN-2016-2188 CONACYT. This paper is scientific product no.1 within the agreement that was recently stipulated between INGV and CICESE. We thank the INGV-Palermo for providing scientific and analytical support. Special thanks are provided to Mariano Tantillo for measuring the noble gas isotopes, Ygor Oliveri for analyzing the stable isotopes of CO<sub>2</sub> and methane, and Francesco Salerno and Mauro Martelli for analyzing the gas chemistry. We also thank PhD Arturo Martín Barajas and PhD Luis Delgado Argote from the Earth Science Division in CICESE, who realize adequate comments about the geology of Baja California. The highly qualified native speaking editors at American Journal Experts edited the manuscript for proper English language. We thank the Editor Marie Edmonds for handling the manuscript and giving suggestions, and Salvatore Inguaggiato and two anonymous reviewers for their comments that greatly improved the manuscript. All the data used are listed in Tables and , in the references, and in Table S2 of the supporting information.

Finally, this study offers the base for a future evaluating the geothermal energy potential of the BCP for a possible exploitation, highlighting the Las Tres Virgenes volcanic zone, specifically the Agua Agria zone, and San Luis Gonzaga Island. To strengthen our knowledge regarding the mantle contribution in the entire peninsula, we note the necessity of acquiring more geochemical data in zones where gas emissions are unknown or poorly studied, such as the southern peninsula from Bahía Concepción to Los Cabos and along the coast of Sonora. In turn, researchers should sample the submarine gases that are emitted in the Wagner and Consag basins, in which the nature of the crust and the origin of the hydrothermal systems are widely debated.

#### References

- Álvarez, R. J. (1995). Reconocimiento geotérmico del noreste de la Península de Baja California proyecto Puertecitos, Reporte de avance, *Internal Report*, Comisión Federal de Electricidad, Residencia General de Cerro Prieto, Residencia de Estudios, Cerro Prieto, México, 15 pp.
- Anderson, D. L. (2007). *New theory of the Earth*. (p. 340). Cambridge: Cambridge University Press. <https://doi.org/10.1017/CBO9781139167291>
- Atwater, T. M. (1970). Implications of plate tectonics for the Cenozoic tectonic evolution of western North America. *Geological Society of America Bulletin*, 81(12), 3513–3536. [https://doi.org/10.1130/0016-7606\(1970\)81\[3513:IOPTFT\]2.0.CO;2](https://doi.org/10.1130/0016-7606(1970)81[3513:IOPTFT]2.0.CO;2)
- Barragán, R. M., Birkle, P., Portugal, E., Arellano, V. M., & Álvarez, J. (2001). Geochemical survey of medium temperature geothermal resources from the Baja California Peninsula and Sonora, México. *Journal of Volcanology and Geophysical Research*, 110(1-2), 101–119. [https://doi.org/10.1016/S0377-0273\(01\)00205-0](https://doi.org/10.1016/S0377-0273(01)00205-0)
- Bernard, B. B., Brooks, J. M., & Sackett, W. M. (1978). *A geochemical model for characterization of hydrocarbon gas sources in marine sediments*, (pp. 435–438). Houston, USA: Offshore Technology Conference.
- Birkle, P., Marin, E., Pinti, D. L., & Castro, C. (2016). Origin and evolution of geothermal fluids from Las Tres Virgenes and Cerro Prieto fields, México-co-genetic volcanic activity and paleoclimatic constraints. *Applied Geochemistry*, 65(November), 36–53. <https://doi.org/10.1016/j.apgeochem.2015.10.009>
- Calmus, T., Pallares, C., Maury, R. C., Aguillón-Robles, A., Bellon, H., Benoit, M., & Michaud, F. (2011). Volcanic markers of the post-subduction evolution of Baja California and Sonora, México: Slab tearing versus lithospheric rupture of the Gulf of California. *Pure Apply Geophysics*, 168(8–9), 1303–1330. <https://doi.org/10.1007/s00024-010-0204-z>
- Cao, M. J., Qin, K. Z., Li, G. M., Evans, N. J., & Jin, L. Y. (2014). Abiogenic Fischer-Tropsch synthesis of methane at the Baogutu reduced porphyry copper deposit, western Junggar, NW-China. *Geochimica et Cosmochimica Acta*, 141, 179–198. <https://doi.org/10.1016/j.gca.2014.06.018>

- Capra, L., Macías, J. L., Espíndola, J. M., & Siebe, C. (1998). Holocene plinian eruption of La Virgen volcano, Baja California, México. *Journal of Volcanology and Geophysical Research*, 80(3–4), 239–266. [https://doi.org/10.1016/S0377-0273\(97\)00049-8](https://doi.org/10.1016/S0377-0273(97)00049-8)
- Caracausi, A., Favara, R., Italiano, F., Nuccio, P. M., Paonita, A., & Rizzo, A. (2005). Active geodynamics of the central Mediterranean Sea: Tensional tectonic evidences in western Sicily from mantle-derived helium. *Geophysical Research Letters*, 32, L04312. <https://doi.org/10.1029/2004GL021608>
- Caracausi, A., Italiano, F., Nuccio, P. M., Paonita, A., & Rizzo, A. (2003). Evidence of deep magma degassing and ascent by geochemistry of peripheral gas emissions at Mount Etna (Italy): Assessment of the magmatic reservoir pressure. *Journal of Geophysical Research*, 108(B10), 2463. <https://doi.org/10.1029/2002JB002095>
- Caracausi, A., & Paternoster, M. (2015). Radiogenic helium degassing and rock fracturing: A case study of the southern Apennines active tectonic region. *Journal of Geophysical Research: Solid Earth*, 120, 2200–2211. <https://doi.org/10.1002/2014JB011462>
- Castillo, P. R., Hawkins, J. W., Lonsdale, P. F., Hilton, D. R., Shaw, A. M., & Glascock, M. D. (2002). Petrology of Alarcon Rise lavas, Gulf of California: Nascent intracontinental ocean crust. *Journal of Geophysical Research*, 107(B10), 2222. <https://doi.org/10.1029/2001JB000666>
- Charlou, J. L., & Donval, J. P. (1993). Hydrothermal methane venting between 12°N and 26°N along the Mid-Atlantic Ridge. *Journal of Geophysical Research*, 98(B6), 9625–9642. <https://doi.org/10.1029/92JB02047>
- Clark, I. D., & Fritz, P. (1997). *Environmental isotopes in hydrogeology*, (p. 328). Boca Raton, Florida, FL: CRC Press/Lewis Publishers.
- Clarke, W. B., Jenkins, W. J., & Top, Z. (1976). Determination of tritium by mass spectrometric measurement of <sup>3</sup>He. *International Journal of Applied Radiation and Isotopes*, 27(9), 515–522. [https://doi.org/10.1016/0020-708X\(76\)90082-X](https://doi.org/10.1016/0020-708X(76)90082-X)
- Coleman, D. D., Risatti, J. B., & Schoell, M. (1981). Fractionation of carbon and hydrogen isotopes by methane-oxidizing bacteria. *Geochimica et Cosmochimica Acta*, 45(7), 1033–1037. [https://doi.org/10.1016/0016-7037\(81\)90129-0](https://doi.org/10.1016/0016-7037(81)90129-0)
- Condie, K. C. (2005). *Earth as an evolving planetary system*, (Second ed. p. 482). Amsterdam, Netherlands: Elsevier.
- Correale, A., Rizzo, A. L., Barry, P. H., Lu, J., & Zheng, J. (2016). Refertilization of lithospheric mantle beneath the Yangtze craton in south-east China: Evidence from noble gases geochemistry. *Gondwana Research*, 38, 289–303. <https://doi.org/10.1016/j.gr.2016.01.003>
- Des Marais, D. J., & Moore, J. G. (1984). Carbon and its isotopes in mid-oceanic basaltic glasses. *Earth and Planetary Science Letters*, 69(1), 43–57. [https://doi.org/10.1016/0012-821X\(84\)90073-6](https://doi.org/10.1016/0012-821X(84)90073-6)
- Des Marais, D. J., Stallard, M. L., Nehring, N. L., & Truesdell, A. H. (1988). Carbon isotope geochemistry of hydrocarbons in the Cerro Prieto geothermal field, Baja California Norte, México. *Chemical Geology*, 71(1–3), 159–167. [https://doi.org/10.1016/0009-2541\(88\)90112-X](https://doi.org/10.1016/0009-2541(88)90112-X)
- Dubacq, B., Bickle, M. J., Wigley, M., Kampman, N., Ballentine, C. J., & Sherwood-Lollar, B. (2012). Noble gas and carbon isotopic evidence for CO<sub>2</sub>-driven silicate dissolution in a recent natural CO<sub>2</sub> field. *Earth and Planetary Science Letters*, 341–344, 10–19. <https://doi.org/10.1016/j.epsl.2012.05.040>
- Espinoza-Ojeda, O. M., Prol-Ledesma, R. M., Iglesias, E. R., & Figueroa-Soto, A. (2017). Update and review of heat flow measurements in México. *Energy*, 121(2017), 466–479. <https://doi.org/10.1016/j.energy.2017.01.045>
- Etiopie, G., Feyzullayev, A., & Baciú, C. L. (2009). Terrestrial methane seeps and mud volcanoes: A global perspective of gas origin. *Marine and Petroleum Geology*, 26(3), 333–344. <https://doi.org/10.1016/j.marpetgeo.2008.03.001>
- Etiopie, G., & Schoell, M. (2014). Abiotic gas: Atypical, but not rare. *Elements*, 10(4), 291–296. <https://doi.org/10.2113/gselements.10.4.291>
- Etiopie, G., & Sherwood-Lollar, B. (2013). Abiotic methane on Earth. *Reviews of Geophysics*, 51, 276–299. <https://doi.org/10.1002/rog.20011>
- Fanale, F. P. (1971). A case for catastrophic early degassing of the Earth. *Chemical Geology*, 8(2), 79–105. [https://doi.org/10.1016/0009-2541\(71\)90051-9](https://doi.org/10.1016/0009-2541(71)90051-9)
- Faure, G., & Mensing, T. M. (2005). *Isotopes, principles and applications*, (Third ed. p. 928). New Jersey, NJ: John Wiley and Sons, Inc., Hoboken.
- Fenby, S., & Gastil, G. (1991). Geologic-tectonic map of the Gulf of California and surrounding areas. In P. Dauphin, & B. Simoneit (Eds.), *The Gulf and Peninsular Province of the Californias* (Chap. 6, pp. 79–83). American Association of Petroleum Geologists.
- Fernández, A., & Pérez-Campos, X. (2017). Lithosphere thickness in the Gulf of California region. *Tectonophysics*, 719–720, 17–26. <https://doi.org/10.1016/j.tecto.2017.06.016>
- Fernandez-Prini, R., Alvarez, J. L., & Harvey, A. H. (2003). Henry's Constants and vapor-liquid distribution constants for gaseous solutes in H<sub>2</sub>O and D<sub>2</sub>O at high temperatures. *Journal of Physical and Chemical Reference Data*, 32(2), 903–916. <https://doi.org/10.1063/1.1564818>
- Forrest, M. J., Ledesma-Vázquez, J., Ussler, W., Kulongoski, J., Hilton, D. R., & Greene, H. G. (2005). Gas geochemistry of a shallow sub-marine hydrothermal vent associated with the El Requesón fault zone, Bahía Concepción, Baja California Sur, México. *Chemical Geology*, 224(1–3), 82–95. <https://doi.org/10.1016/j.chemgeo.2005.07.015>
- Galimov, E. M., & Simoneit, B. R. T. (1982). Geochemistry of interstitial gases in sedimentary deposits of the Gulf of California, Deep Sea Drilling Project Leg 64. In J. R. Curran, & D. G. Moore (Eds.), *Initial reports of the Deep Sea Drilling Project*, (Vol. 64, pp. 781–788). Washington, D.C.: U.S. Government Printing Office. <https://doi.org/10.2973/dsdp.proc.64.124.1982>
- García-Sánchez, L., Macías, J. L., Sosa-Ceballos, G., Arce, J. L., Garduño-Monroy, V. H., Saucedo, R., et al. (2017). Genesis and evolution of the Cerro Prieto volcanic complex, Baja California, México. *Bulletin of Volcanology*, 79(6). <https://doi.org/10.1007/s00445-017-1126-8>
- Garduño-Monroy, V. H., Vargas-Ledezma, H., & Campos, J. O. (1993). Preliminary geologic studies of Sierra El Aguajito (Baja California, México): A resurgent-type caldera. *Journal of Volcanology and Geothermal Research*, 59(1–2), 47–58. [https://doi.org/10.1016/0377-0273\(93\)90077-5](https://doi.org/10.1016/0377-0273(93)90077-5)
- Giggenbach, W. F. (1992). The composition of gases in geothermal and volcanic systems as a function of tectonic setting. In Y. K. Kharaka, & A. S. Maest (Eds.), *Water-rock interaction*, (Vol. 2, pp. 873–878). Rotterdam: Balkema.
- Gillfillan, S. M. V., Sherwood-Lollar, B., Holland, G., Blagburn, D., Stevens, S., Schoell, M., et al. (2009). Solubility trapping in formation water as dominant CO<sub>2</sub> sink in natural gas fields. *Nature*, 458(7238), 614–618. <https://doi.org/10.1038/nature07852>
- González-Escobar, M., Suárez-Vidal, F., Sojo-Amezquita, A., Gallardo-Mata, C. G., & Martín-Barajas, A. (2014). Consag basin: Northern Gulf of California, evidence of generation of new crust, based on seismic reflection data. *International Geology Review*, 56(11), 1315–1331. <https://doi.org/10.1080/00206814.2014.941023>
- González-Fernández, A., Danobeitia, J. J., Delgado-Argote, L. A., Michaud, F., Cordoba, D., & Bartolomé, R. (2005). Mode of extension and rifting history of upper Tiburon and upper Delfin basin, northern Gulf of California. *Journal of Geophysical Research*, 110, B01313. <https://doi.org/10.1029/2003JB002941>
- Graham, D. W. (2002). Noble gas isotope geochemistry of mid-ocean ridge and ocean island basalts: Characterization of mantle source reservoirs. In D. Porcelli, C. J. Ballentine, & R. Wieler (Eds.), *Noble gases in geochemistry and cosmochemistry, Reviews in mineralogy and geochemistry*, (Vol. 47, pp. 245–317). Washington, DC: The Mineralogical Society of America.

- Grassa, F., Capasso, G., Oliveri, Y., Sollami, A., Carreira, P., Rosário Carvalho, M., et al. (2010). Nitrogen isotopes determination in natural gas: Analytical method and first results on magmatic, hydrothermal and soil gas samples. *Isotopes in Environmental and Health Studies*, 46(2), 141–155. <https://doi.org/10.1080/10256016.2010.491914>
- Gülec, N., Hilton, D. R., & Mutlu, H. (2002). Helium isotope variations in Turkey: Relationship to tectonics, volcanism and recent seismic activities. *Chemical Geology*, 187(1–2), 129–142. [https://doi.org/10.1016/S0009-2541\(02\)00015-3](https://doi.org/10.1016/S0009-2541(02)00015-3)
- Han, L., Hole, J. A., Stock, J. M., Fuis, J. S., Kell, A., Driscoll, N. W., et al. (2016). Continental rupture and the creation of new crust in the Salton trough rift, Southern California and northern México: Results from the Salton seismic imaging project. *Journal of Geophysical Research: Solid Earth*, 121, 7469–7489. <https://doi.org/10.1002/2016JB013139>
- Hausback, B., Cook, A., Farrar, C. D., Giambastiani, M., Martin, A., Paz-Moreno, A., et al. (2003). Isla San Luis volcano, Baja California, México; Late Holocene eruptions, In *99th Annual Meeting of the Cordilleran Section, Geological Society of America* (Vol.35, pp. 29), Puerto Vallarta, México.
- Herzig, C. T. (1990). Geochemistry of igneous rocks from the Cerro Prieto geothermal field, northern Baja California, México. *Journal of Volcanology and Geothermal Research*, 42(3), 261–271. [https://doi.org/10.1016/0377-0273\(90\)90003-X](https://doi.org/10.1016/0377-0273(90)90003-X)
- Herzig, C. T., & Elders, W. A. (1988). Nature and significance of igneous rocks cored in the State 2-14 research borehole, Salton Sea scientific drilling project, California. *Journal of Geophysical Research*, 93(B11), 13,069–13,080. <https://doi.org/10.1029/JB093iB11p13069>
- Hilton, D. R., Fisher, T. P., & Marty, B. (2002). Noble gases and volatile recycling at subduction zones. *Reviews in Mineralogy and Geochemistry*, 47(1), 319–370. <https://doi.org/10.2138/rmg.2002.47.9>
- Hrubcová, P., Geissler, W. H., Bräuer, K., Vavryčuk, V., Tomek, Č., & Kämpf, H. (2017). Active magmatic underplating in western Eger rift, central Europe. *Tectonics*, 36, 2846–2862. <https://doi.org/10.1002/2017TC004710>
- Ichinose, G., Day, S., Magistrale, H., Prush, T., Vernon, F., & Edelman, A. (1996). Crustal thickness variations beneath the peninsular ranges, Southern California. *Geophysical Research Letters*, 23(22), 3095–3098. <https://doi.org/10.1029/96GL03020>
- INEGI (2013). Conjunto de datos vectoriales de Geología Escala 1:250 000, (Capa Fallas y Fracturas). official site <http://www.inegi.org.mx>
- Inguaggiato, C., Censi, P., D'Alessandro, W., & Zuddas, P. (2016). Geochemical characterization of gases along the Dead Sea rift: Evidences of mantle-CO<sub>2</sub> degassing. *Journal of Volcanology and Geothermal Research*, 320, 50–57. <https://doi.org/10.1016/j.jvolgeores.2016.04.008>
- Jambon, A., Weber, H. W., & Begemann, F. (1985). Helium and argon from an Atlantic MORB glass: Concentration, distribution and isotopic composition. *Earth and Planetary Science Letters*, 73(2–4), 255–268. [https://doi.org/10.1016/0012-821X\(85\)90074-3](https://doi.org/10.1016/0012-821X(85)90074-3)
- Javoy, M., Pineau, F., & Delorme, H. (1986). Carbon and nitrogen isotopes in the mantle. In S. Deutsch & A.W. Hofmann (Eds.), *Isotopes in Geology-Picciotto. Chemical Geology*, 57(1–2), 41–62 (special issue). [https://doi.org/10.1016/0009-2541\(86\)90093-8](https://doi.org/10.1016/0009-2541(86)90093-8)
- Kurz, M. D., Jenkins, W. J., & Hart, S. R. (1982). Helium isotopic systematics of oceanic islands and mantle heterogeneity. *Nature*, 297(5861), 43–47. <https://doi.org/10.1038/297043a0>
- Lewis, J. L., Day, S. M., Magistrale, H., Castro, R. R., Astiz, L., Rebolgar, C., et al. (2001). Crustal thickness of the Peninsular Ranges and gulf extensional province in the Californias. *Journal of Geophysical Research*, 106(B7), 13,599–13,611. <https://doi.org/10.1029/2001JB000178>
- Lewis, J. L., Day, S. M., Magistrale, H., Eakins, J., & Vernon, F. (2000). Regional crustal thickness variations of the Peninsular Ranges, Southern California. *Geology*, 28(4), 303–306. [https://doi.org/10.1130/0091-7613\(2000\)28<303:RCTVOT>2.0.CO;2](https://doi.org/10.1130/0091-7613(2000)28<303:RCTVOT>2.0.CO;2)
- Linn, M. S. (1978). *Coastal warm spring systems northeastern Baja California, (Master's thesis)*, (p. 217). San Diego: San Diego State University. <http://hdl.handle.net/10211.3/185037>
- Lizarralde, D., Axen, G. J., Brown, H. E., Fletcher, J. M., González-Fernández, A., Harding, A. J., & Umhoefer, P. J. (2007). Variation in styles of rifting in the Gulf of California. *Nature*, 448(7152), 466–469. <https://doi.org/10.1038/nature06035>
- Lizarralde, D., Soule, S. A., Seewald, J. S., & Proskurovski, G. (2010). Carbon release by off-axis magmatism in a young sedimented spreading center. *Nature Geoscience*, 4(1), 50–54. <https://doi.org/10.1038/ngeo1006>
- Lonsdale, P., & Becker, K. (1985). Hydrothermal plumes, hot springs, and conductive heat flow in the southern trough of Guaymas basin. *Earth and Planetary Science Letters*, 73(2–4), 211–225. [https://doi.org/10.1016/0012-821X\(85\)90070-6](https://doi.org/10.1016/0012-821X(85)90070-6)
- Lonsdale, P. F. (1989). Geology and tectonic history of the Gulf of California. In E. L. Winterer, D. M. Hussong, & R. W. Decker (Eds.), *The eastern Pacific Ocean and Hawaii*, (pp. 499–521). Boulder, Colorado: Geological Society of America.
- López, A., Casarrubias, Z., & Leal, R. (1993). Estudio geológico regional de la zona geotérmica de Las Tres Virgenes. *Internal Report*, OGL-BC-002/93, GPG-CFE, 102 pp.
- López, A., Robin, C., Cantagrel, J.M., & Vincent, P. (1989). Estudio geoquímico, mineralógico y edades radiométricas de la zona de Tres Virgenes, B.C.S. implicaciones geotérmicas. *Internal Report*, 5/89, GPG-CFE, 50 pp.
- Lupton, J. E. (1979). Helium-3 in the Guaymas basin: Evidence for injection of mantle volatiles in the Gulf of California. *Journal of Geophysical Research*, 84(B13), 7446–7452. <https://doi.org/10.1029/JB084iB13p07446>
- Mabry, J., Lan, T., Burnard, P., & Marty, B. (2013). High-precision helium isotope measurements in air. *Journal of Analytical Atomic Spectrometry*, 28(12), 1903–1910. <https://doi.org/10.1039/c3ja50155h>
- Mamyrin, B. A., Anufriev, G. S., Kamensky, I., & Tolstikhin, I. N. (1970). Determination of the isotopic composition of atmospheric helium. *Geochemistry International*, 7, 498–505.
- Mamyrin, B. A., & Tolstikhin, I. N. (1984). *Helium isotopes in nature*, (p. 273). New York: Elsevier.
- Martin-Barajas, A., González-Escobar, M., Fletcher, J. M., Pacheco, M., Oskin, M., & Dorsey, D. (2013). Thick deltaic sedimentation and detachment faulting delay the onset of continental rupture in the northern Gulf of California: Analysis of seismic reflection profiles. *Tectonics*, 32, 1294–1311. <https://doi.org/10.1002/tect.20063>
- Martin-Barajas, A., Stock, J. M., Layer, P., Hausback, B., Renne, P., & López-Martínez, M. (1995). Arc-rift transition volcanism in the Puertecitos volcanic province, northeastern Baja California, México. *Geological Society American Bulletin*, 107(4), 407–424. [https://doi.org/10.1130/0016-7606\(1995\)107<0407:ARTVIT>2.3.CO;2](https://doi.org/10.1130/0016-7606(1995)107<0407:ARTVIT>2.3.CO;2)
- Martin-Barajas, A., Weber, B., Schmitt, A.K., & Lonsdale, P. (2008). Recent rift volcanism in the northern Gulf of California and the Salton trough: Why a preponderance of evolved magmas?. *Fall AGU Meeting*, San Francisco, Dic. 15-19, Abstract T11A-1841.
- Marty, B., & Jambon, A. (1987). C<sup>3</sup>He in volatile flux from the solid Earth: Implications for carbon dynamics. *Earth and Planetary Science Letters*, 83(1–4), 16–26. [https://doi.org/10.1016/0012-821X\(87\)90047-1](https://doi.org/10.1016/0012-821X(87)90047-1)
- Marty, B., Jambon, A., & Sano, Y. (1989). Helium isotopes and CO<sub>2</sub> in volcanic gases in Japan. *Chemical Geology*, 76(1–2), 25–40. [https://doi.org/10.1016/0009-2541\(89\)90125-3](https://doi.org/10.1016/0009-2541(89)90125-3)
- Mazor, E., & Truesdell, A. H. (1984). Dynamics of a geothermal field traced by noble gases: Cerro Prieto, México. *Geothermics*, 13(1–2), 91–102. [https://doi.org/10.1016/0375-6505\(84\)90009-9](https://doi.org/10.1016/0375-6505(84)90009-9)

- Mazzini, A., Svensen, H., Etiope, E., Onderdonk, N., & Banks, D. (2011). Fluid origin, gas fluxes and plumbing system in the sediment-hosted Salton Sea Geothermal System (California, USA). *Journal of Volcanology and Geothermal Research*, 205(3–4), 67–83. <https://doi.org/10.1016/j.jvolgeores.2011.05.008>
- McCullom, T. M., & Seewald, J. S. (2007). Abiotic synthesis of organic compounds in deep-sea hydrothermal environments. *Chemical Reviews*, 107(2), 382–401. <https://doi.org/10.1021/cr0503660>
- Merlivat, L., Pineau, F., & Javoy, M. (1987). Hydrothermal vent waters at 13-degrees-N on the East Pacific Rise-isotopic composition and gas concentration. *Earth and Planetary Science Letters*, 84(1), 100–108. [https://doi.org/10.1016/0012-821X\(87\)90180-4](https://doi.org/10.1016/0012-821X(87)90180-4)
- Monterey Bay Aquarium Research Institute (2012). Cruise report: Leg 7: Volcanoes and seamounts April 21-May 1. [http://www.mbari.org/expeditions/goc12/legs/leg7/L7\\_index.html](http://www.mbari.org/expeditions/goc12/legs/leg7/L7_index.html)
- Moreira, M. (2013). Noble gas constraints on the origin and evolution of Earth's volatiles. *Geochemical Perspectives*, 2(2), 229–403. <https://doi.org/10.7185/geochempersp.2.2>
- Moreira, M., & Allègre, C. J. (1998). Helium-neon systematics and the structure of the mantle. *Chemical Geology*, 147(1-2), 53–59. [https://doi.org/10.1016/S0009-2541\(97\)00171-X](https://doi.org/10.1016/S0009-2541(97)00171-X)
- Moreira, M., & Sarda, P. (2000). Noble gas constraints on degassing processes. *Earth and Planetary Science Letters*, 176(3–4), 375–386. [https://doi.org/10.1016/S0012-821X\(00\)00010-8](https://doi.org/10.1016/S0012-821X(00)00010-8)
- Morrison, P., & Pine, J. (1955). Radiogenic origin of the helium isotopes in rocks. *Annals of the New York Academy of Sciences*, 62(3), 69–92. <https://doi.org/10.1111/j.1749-6632.1955.tb35366.x>
- Negrete-Aranda, R., Spelz, R.M., Hilton, D.R., Téllez, M., & González-Yahimovich, O. (2015). Mapping mantle-melting anomalies in Baja California: A combined helium-seismology approach. *Fall AGU Meeting*, San Francisco, Dic. 14-18, abstract OS23C-2026.
- Ozima, M., & Podosek, F. A. (1983). *Noble gas geochemistry* (p. 340). New York, NY: Cambridge University Press.
- Paz-Moreno, F. A., & Demant, A. (1999). The recent Isla San Luis volcanic centre: Petrology of a rift-related volcanic suite in the northern Gulf of California, México. *Journal of Volcanology and Geothermal Research*, 93(1–2), 31–52. [https://doi.org/10.1016/S0377-0273\(99\)00083-9](https://doi.org/10.1016/S0377-0273(99)00083-9)
- Persaud, P., Pérez-Campos, X., & Clayton, R. W. (2007). Crustal thickness variations in the margins of the Gulf of California from receiver functions. *Geophysical Journal International*, 170(2), 687–699. <https://doi.org/10.1111/j.1365-246X.2007.03412.x>
- Persaud, P., Stock, J. M., Steckler, M. S., Martín-Barajas, A., Diebold, J. B., González-Fernández, A., & Mountain, G. S. (2003). Active deformation and shallow structure of the Wagner, Consag, and Delfin basins, northern Gulf of California, México. *Journal of Geophysical Research*, 108(B7), 2355. <https://doi.org/10.1029/2002JB001937>
- Pineau, F., & Javoy, M. (1983). Carbon isotopes and concentrations in mid-oceanic ridge basalt. *Earth Planetary Science Letter*, 62(2), 239–257. [https://doi.org/10.1016/0012-821X\(83\)90087-0](https://doi.org/10.1016/0012-821X(83)90087-0)
- Pinti, D., Castro, M. C., López-Hernández, A., Hernández-Hernández, M. A., Richard, L., Chris, M. H., et al. (2018). Cerro Prieto geothermal field (Baja California, Mexico)—A fossil system? Insights from a noble gas study. *Journal of Volcanology and Geothermal Research*, 371, 32–45. <https://doi.org/10.1016/j.jvolgeores.2018.12.010>
- Polyak, B. G., Kononov, V. I., Fernandez, R., Kamenskiy, I. L., & Zinkevich, V. P. (1991). Helium isotopes in thermal fluids of Baja California and adjacent areas. *International Geology Review*, 33(12), 1218–1232. <https://doi.org/10.1080/00206819109465747>
- Polyak, B. G., Prasolov, E. M., Kononov, V. I., Verkhovskiy, A. B., Gonzalez, A., Templos, L. A., et al. (1982). Isotopic composition and concentration of inert gases in Mexican hydrothermal systems. *Geofísica Internacional*, 21(3), 193–227.
- Poreda, R., & Craig, H. (1989). Helium isotope ratios in Circum-Pacific volcanic arcs. *Nature*, 338(6215), 473–478. <https://doi.org/10.1038/338473a0>
- Ramírez-Ramos, E. E., Vidal-Villegas, A., González-Fernández, A., & Stock, J. M. (2015). A crustal velocity model for the southern Mexicali Valley, Baja California, México. *Seismological Research Letters*, 86(1), 1–11. <https://doi.org/10.1785/0220140007>
- Ray, M. C., Hilton, D. R., Muñoz, J., Fischer, T. P., & Shaw, A. M. (2009). The effects of volatile recycling, degassing and crustal contamination on the helium and carbon geochemistry of hydrothermal fluids from the southern volcanic zone of Chile. *Chemical Geology*, 266(1-2), 38–49. <https://doi.org/10.1016/j.chemgeo.2008.12.026>
- Rayleigh, J. W. S. (1896). Theoretical considerations respecting the separation of gases by diffusion and similar processes. *The Philosophical Magazine*, 42, 77–107.
- Reyes, L. M., Rebolgar, C. J., & Castro, R. (2001). Depth of the Moho in northern Baja California using (Pg-Pn) travel times. *Geofísica Internacional*, 40, 1–9.
- Richard, L., Pinti, D. L., Hélie, J. F., López-Hernández, A., Shibata, T., Castro, C. M., et al. (2019). Variability of deep carbon sources in Mexican geothermal fluids. *Journal of Volcanology and Geothermal Research*, 370(2019), 1–12. <https://doi.org/10.1016/j.jvolgeores.2018.11.026>
- Rizzo, A. L., Barberi, F., Carapezza, M. L., Di Piazza, A., Francalanci, L., Sortino, F., & D'Alessandro, W. (2015). New mafic magma refilling a quiescent volcano: Evidence from He-Ne-Ar isotopes during the 2011–2012 unrest at Santorini, Greece. *Geochemistry, Geophysics, Geosystems*, 16, 798–814. <https://doi.org/10.1002/2014GC005653>
- Rizzo, A. L., Caracausi, A., Chavagnac, V., Nomikou, P., Polymenakou, P. N., Mandalakis, M., & Lampridou, D. (2016). Kolumbo submarine volcano (Greece): An active window into the Aegean subduction system. *Scientific Reports*, 6(1), 28013. <https://doi.org/10.1038/srep28013>
- Robinson, P. T., Elders, W. A., & Muffler, L. J. P. (1976). Quaternary volcanism in the Salton Sea geothermal field, Imperial Valley, California. *Geological Society American Bulletin*, 87(3), 347–360. [https://doi.org/10.1130/0016-7606\(1976\)87<347:QVITSS>2.0.CO;2](https://doi.org/10.1130/0016-7606(1976)87<347:QVITSS>2.0.CO;2)
- Rossetter, R. J. (1970). *Geology of the San Luis and San Lorenzo island groups, Gulf of California, (Master's thesis)* (p. 104). San Diego, CA: San Diego State University. <http://hdl.handle.net/10211.10/193>
- Sano, Y., & Fischer, T. P. (2013). The analysis and interpretation of noble gases in modern hydrothermal systems. In P. Burnard (Ed.), *The noble gases as geochemical tracers*, (pp. 249–317). Berlin Heidelberg: Springer-Verlag. [https://doi.org/10.1007/978-3-642-28836-4\\_10](https://doi.org/10.1007/978-3-642-28836-4_10)
- Sano, Y., & Marty, B. (1995). Origin of carbon in fumarolic gases from island arcs. *Chemical Geology*, 119(1-4), 265–274. [https://doi.org/10.1016/0009-2541\(94\)00097-R](https://doi.org/10.1016/0009-2541(94)00097-R)
- Sano, Y., Takahata, N., & Seno, T. (2006). Geographical distribution of <sup>3</sup>He/<sup>4</sup>He ratios in the Chugoku District, southwestern Japan. *Pure and Applied Geophysics*, 167, 745–757. <https://doi.org/10.1007/s00024-006-0035-0>
- Sano, Y., Tokutake, T., & Takahata, N. (2008). Accurate measurement of atmospheric helium isotopes. *Analytical Sciences: The International Journal of the Japan Society for Analytical Chemistry*, 24(4), 521–525. <https://doi.org/10.2116/analsci.24.521>
- Sano, Y., & Wakita, H. (1985). Geographical distribution of <sup>3</sup>He/<sup>4</sup>He ratios in Japan: Implications for arc tectonics and incipient magmatism. *Journal of Geophysical Research*, 90(B10), 8729–8741. <https://doi.org/10.1029/JB090iB10p08729>



- Sano, Y., & Williams, S. N. (1996). Fluxes of mantle and subducted carbon along convergent plate boundaries. *Geophysical Research Letters*, 23(20), 2749–2752. <https://doi.org/10.1029/96GL02260>
- Schmitt, A. K., Martin, A., Stockli, D. F., Farley, K. A., & Lovera, O. M. (2012). (U-Th)/He zircon and archaeological ages for a late prehistoric eruption in the Salton trough (California, USA). *Geology*, 41(1), 7–10. <https://doi.org/10.1130/G33634.1>
- Schmitt, A. K., Martin, A., Weber, B., Stockli, D. F., Zou, H., & Shen, C. C. (2013). Oceanic magmatism in sedimentary basins of the northern Gulf of California rift. *Bulletin of the Geological Society of America*, 125(11–12), 1833–1850. <https://doi.org/10.1130/B30787.1>
- Schmitt, A. K., Stockli, D. F., Niedermann, S., Lovera, O. M., & Hausback, B. P. (2010). Eruption ages of Las Tres Virgenes volcano (Baja California): A tale of two helium isotopes. *Quaternary Geochronology*, 5(5), 503–511. <https://doi.org/10.1016/j.quageo.2010.02.004>
- Schoell, M. (1980). The hydrogen and carbon isotopic composition of methane from natural gases of various origins. *Geochimica et Cosmochimica Acta*, 44(5), 649–661. [https://doi.org/10.1016/0016-7037\(80\)90155-6](https://doi.org/10.1016/0016-7037(80)90155-6)
- Schoell, M. (1983). Genetic characterization of natural gases. *American Association of Petroleum Geologists*, 67, 2225–2238. <https://doi.org/10.1306/AD46094A-16F7-11D7-8645000102C1865D>
- Schoell, M. (1988). Multiple origins of methane in the Earth. *Chemical Geology*, 71(1–3), 1–10. [https://doi.org/10.1016/0009-2541\(88\)90101-5](https://doi.org/10.1016/0009-2541(88)90101-5)
- Spelz, R.M., Lupton, J.E., Evans, L.J., Zierenberg, A., Clague, D.A., Neumann, F., & Paduan, J.B. (2015). Noble gas geochemistry of the newly discovered hydrothermal fields in the Gulf of California: Preliminary He-isotope ratios from the Alarcon Rise and Pescadero basin vent sites. *Fall AGU Meeting*, San Francisco, Dec. 14–18, Abstract OS23C-2028.
- Stock, J. M., & Hodges, K. V. (1989). Pre-Pliocene extension around the Gulf of California and the transfer of Baja California to the Pacific plate. *Tectonics*, 8(1), 99–115. <https://doi.org/10.1029/TC008i001p00099>
- Stock, J. M., & Lee, J. (1994). Do microplates in subduction zones leave a geological record? *Tectonics*, 13(6), 1472–1487. <https://doi.org/10.1029/94TC01808>
- Tajika, E. (1998). Mantle degassing of major and minor volatile elements during the Earth's history. *Geophysical Research Letters*, 25(21), 3991–3994. <https://doi.org/10.1029/1998GL900106>
- Tardani, D., Reich, M., Rouilleau, E., Takahata, N., Sano, Y., Pérez-Flores, P., et al. (2016). Exploring the structural controls on helium, nitrogen and carbon isotope signatures in hydrothermal fluids along an intra-arc fault system. *Geochimica et Cosmochimica Acta*, 184(2016), 193–211.
- Truesdell, A., Rye, R.O., Pearson, F.J., Olson, E.R., Nehring, N.L., Huebner, M.A., & Coplen, T.B. (1978). Preliminary isotopic studies of fluids from the Cerro Prieto Geothermal Field, Baja California, México. *Proceedings, 1st Symposium on the Cerro Prieto Geothermal Field, Baja California, México*, San Diego. LBL Report 7098.
- Trull, T., Nadeau, S., Pineau, F., Polvé, M., & Javoy, M. (1993). C-He systematics in for mantle carbon hotspot xenoliths: Implications contents and carbon recycling. *Earth and Planetary Science Letters*, 118(1–4), 43–64. [https://doi.org/10.1016/0012-821X\(93\)90158-6](https://doi.org/10.1016/0012-821X(93)90158-6)
- U.S. Geological Survey (2006). Quaternary fault and fold database for the United States, accessed 2015, from USGS web site: <http://earthquakes.usgs.gov/regional/qfaults>
- Umeda, K., Sakagawa, Y., Ninomiya, A., & Asamori, K. (2007). Relationship between helium isotopes and heat flux from hot springs in a non-volcanic region, Kii Peninsula, Southwest Japan. *Geophysical Research Letters*, 34, L05310. <https://doi.org/10.1029/2006GL028975>
- Vidal, F. V., Welhan, J., & Vidal, V. M. (1982). Stable isotopes of helium, nitrogen and carbon in a coastal submarine hydrothermal system. *Journal of Volcanology and Geothermal Research*, 12(1–2), 101–110. [https://doi.org/10.1016/0377-0273\(82\)90006-3](https://doi.org/10.1016/0377-0273(82)90006-3)
- Vidal, V. M., Vidal, F. V., & Isaacs, J. D. (1981). Coastal submarine hydrothermal activity off northern Baja California 2. Evolutionary history and isotope geochemistry. *Journal of Geophysical Research*, 86(B10), 9451–9468. <https://doi.org/10.1029/JB086iB10p09451>
- Vogel, J. C. (1970). *Carbon-14 dating of groundwater. isotope hydrology*, (pp. 225–237). Vienna: International Atomic Energy Agency.
- Von Damm, K. L., Edmond, J. M., Grant, B., & Measures, C. I. (1985). Chemistry of submarine hydrothermal solutions at Guaymas basin, Gulf of California. *Geochimica et Cosmochimica Acta*, 49(11), 2221–2237. [https://doi.org/10.1016/0016-7037\(85\)90223-6](https://doi.org/10.1016/0016-7037(85)90223-6)
- Wakita, H., Sano, Y., & Mizoue, M. (1987). High <sup>3</sup>He emanation and seismic swarms observed in a nonvolcanic, forearc region. *Journal of Geophysical Research*, 92(B12), 12,539–12,546. <https://doi.org/10.1029/JB092iB12p12539>
- Welhan, J. A. (1981). *Carbon and hydrogen gases in hydrothermal systems: The search for a mantle source. (Doctoral Thesis)*, (p. 194). San Diego, California: University of California.
- Welhan, J. A. (1988). Origins of methane in hydrothermal systems. *Chemical Geology*, 71(1–3), 183–198. [https://doi.org/10.1016/0009-2541\(88\)90114-3](https://doi.org/10.1016/0009-2541(88)90114-3)
- Welhan, J. A., & Craig, H. (1982). Abiogenic methane in mid-ocean ridge hydrothermal fluids. In W. J. Gwilliam (Ed.), *Deep Source Gas Workshop Tech. Proc.* (pp. 122–128). Morgantown, West Virginia.
- Welhan, J. A., & Craig, H. (1983). Methane, hydrogen and helium in hydrothermal fluids of 21°N on the East Pacific Rise. In P. A. Rona, K. Boström, L. Laubier, & K. L. Smith, Jr. (Eds.), *Hydrothermal Processes at Seafloor Spreading Centers* (pp. 391–409). New York, NY: Plenum. [https://doi.org/10.1007/978-1-4899-0402-7\\_17](https://doi.org/10.1007/978-1-4899-0402-7_17)
- Welhan, J. A., & Lupton, J. E. (1987). Light hydrocarbon gases in Guaymas basin hydrothermal fluids: Thermogenic versus abiogenic origin. *American Association of Petroleum Geologists*, 71(2), 215–223.
- Welhan, J. A., Poreda, R., Lupton, J. E., & Craig, H. (1978). Gas chemistry and helium isotopes at Cerro Prieto. *Geothermics*, 8(3–4), 241–244. [https://doi.org/10.1016/0375-6505\(79\)90046-4](https://doi.org/10.1016/0375-6505(79)90046-4)
- Wen, H. Y., Sano, Y., Takahata, N., Tomonaga, Y., Ishida, A., Tanaka, K., et al. (2016). Helium and methane sources and fluxes of shallow submarine hydrothermal plumes near the Tokara Islands, southern Japan. *Scientific Reports*, 6(1), 1–9. <https://doi.org/10.1038/srep34126>
- Whiticar, M. J. (1999). Carbon and hydrogen isotope systematics of bacterial formation and oxidation of methane. *Chemical Geology*, 161(1–3), 291–314. [https://doi.org/10.1016/S0009-2541\(99\)00092-3](https://doi.org/10.1016/S0009-2541(99)00092-3)
- Wright, H. M., Vazquez, J. A., Champion, D. E., Calvert, A. T., Mangan, M. T., Stelten, M., et al. (2015). Episodic Holocene eruption of the Salton buttes rhyolites, California, from paleomagnetic, U-Th, and Ar/Ar dating. *Geochemistry, Geophysics, Geosystems*, 18, 1541–1576. <https://doi.org/10.1002/2014GC005684>.Key
- Zhang, J., Quay, P. D., & Wilbur, & D.O. (1995). Carbon isotope fractionation during gas-water exchange and dissolution of CO<sub>2</sub>. *Geochimica et Cosmochimica Acta*, 59(1), 107–114. [https://doi.org/10.1016/0016-7037\(95\)91550-D](https://doi.org/10.1016/0016-7037(95)91550-D)